EPITAXIAL GROWTH OF SILICON CARBIDE ON ON-AXIS SILICON CARBIDE SUBSTRATES USING METHYLTRICHLOROSILANE CHEMICAL VAPOR DEPOSITION

by

KYLE SWANSON

B.S. Kansas State University, 2006

A THESIS

submitted in partial fulfillment of the requirements for the degree

MASTER OF SCIENCE

Department of Chemical Engineering
College of Engineering

KANSAS STATE UNIVERSITY
Manhattan, Kansas
2008

Approved by:

Major Professor
James Edgar, PhD

Copyright

KYLE SWANSON

2008

Abstract

4H-silicon carbide (4H-SiC) is a wide bandgap semiconductor with outstanding capabilities for high temperature, high power, and high frequency electronic device applications. Advances in its processing technology have resulted in large micropipe-free single crystals and high speed epitaxial growth on off-axis silicon face substrates. Extraordinarily high growth rates of high quality epitaxial films (>100 μm per hour) have been achieved, but only on off-axis substrates (misoriented 4° to 8° from the (0001) crystallographic plane). There is a strong incentive to procure an on-axis growth procedure, due to the excessive waste of high quality single crystal associated with wafering off-axis substrates.

The purpose of this research was to develop a reliable process for homoepitaxial growth of 4H-SiC on on-axis 4H-SiC. Typically the use of on-axis SiC for epitaxial growth is undesired due to the increased probability of 3C-SiC inclusions and polycrystalline growth. However, it is believed that the presence of chlorine during reaction may reduce the presence of 3C-SiC and improve the quality of the epitaxial film. Therefore homoepitaxial SiC was deposited using methyltrichlorosilane (MTS) and ethane sources with carrier gases consisting of argon-hydrogen mixtures. Ethane was used to increase the C/Si ratio, to aid in the prevention of 3C-SiC, and to help eliminate silicon droplets deposited during epitaxial growth. Deposition occurred in a homemade, quartz, cold wall chemical vapor deposition reactor.

Epitaxial films on on-axis 4H-SiC were deposited without the presence of 3C-SiC inclusions or polycrystalline SiC, as observed by defect selective etching, scanning electron microscopy and optical microscopy. Large defect free areas, ~5 mm^2, with epitaxial film thicknesses of ~6 μm were grown on on-axis 4H-SiC. Epitaxial films had approximately an 80%, ~20 cm^{-2}, decrease in defect density as compared to the substrates. The growth rate was independent of face polarity and orientation of the substrate. The optimal temperature for hydrogen etching, to promote the smoothest epitaxial films for on-axis substrates (both C- and Si- polarties), is ~1550 °C for 10 minutes in the presence of 2 slm hydrogen. The optimum C/Si ratio for epitaxial growth on on-axis 4H-SiC is 1; excess carbon resulted in the codeposition of graphite and cone-shaped silicon carbide defects.

Table of Contents

List of Figures vi

List of Tables ix

Acknowledgements x

Dedication xi

CHAPTER 1 - The Need for Something New 1

1.1 Structure and Polytypes 1

1.2 Electrical and Physical Properties 4

1.2.1 Electrical Properties 5

1.2.2 Physical Properties 6

1.3 Applications 7

1.4 Growth Chemistry 8

1.4.1 Bulk Crystal Growth 8

1.4.2 Epitaxial Growth 11

CHAPTER 2 - Experimental 16

2.1 Reactor and Heating Element 17

2.2 In-situ Hydrogen Etching 18

2.3 Epitaxial Growth 19

2.4 Defect Selective Etching 19

2.5 Characterization Techniques 20

2.5.1 Atomic Force Microscopy 20

2.5.2 Scanning Electron Microscopy/Energy dispersive spectroscopy 21

2.5.3 Secondary Ion Mass Spectrometry 22

2.5.4 Micro Raman Spectroscopy 23

CHAPTER 3 - Results and Discussion 24

3.1 In-situ Hydrogen Etching 24

3.2 Temperature 28

3.2.1 Growth Rate 28

3.2.2 Surface Morphology 31
3.3 MTS Molar Fraction 32
3.3.1 Growth Rate 32
3.3.2 Surface Morphology 34
3.3.3 SIMS 36
3.4 Defects 37
3.4.1 Defect Selective Etching 37
3.4.2 Silicon Droplets 39
CHAPTER 4 - Conclusion 45
Appendix A - References 46
A.1 Cited Sources 46
A.2 Additional Sources 49
Appendix B - Equipment and Supplies 50
Appendix C - Step By Step Procedure 52
C.1 Sample Preparation 52
C.2 Sample Loading and Purging 52
C.3 Hydrogen Etching 52
C.4 Epitaxial Growth 53

List of Figures

Figure 1.1: Tetrahedral bonding of carbon and silicon atoms in SiC, unit structure can consist as CSi_4 or SiC_4. 1

Figure 1.2: Hexagonal structure of a unit cell for 4H-SiC and 6H-SiC. 2

Figure 1.3: Possible stacking sequence locations in a close-packed crystal structure, perpendicular to the c-axis [0001]; the top right corner shows a carbon-silicon biatomic molecule. 3

Figure 1.4: 3-D view of stacking sequence for 3C-SiC, 4H-SiC and 6H-SiC. 4

Figure 1.5: A) 4H-SiC single crystal boule produced using the modified Lely process; B) Epitaxial layer grown on 4H-SiC with a thickness of ~5 µm. 8

Figure 1.6: Basic diagram of Lely's reactor setup. 9

Figure 1.7: Basic diagram of modified Lely process. 10

Figure 1.8: Two step method proposed by Toyota Central R&D and DENSO Corp., to produce micropipe free SiC.[25] 10

Figure 1.9: Maximum growth rates from multiple references, dating 2005 – 2006, achieved using non-halogenated and halogenated precursors. 13

Figure 1.10: Step growth mechanism shown on 4H-SiC, (Top) Vertical growth on an on-axis substrate, showing 3C-SiC inclusions (ordering CAB and ABC), (Bottom) 4H-SiC step growth on a large off-axis angled substrate, parallel to substrate steps produces the same polytype as the substrate. 14

Figure 2.1: Silicon carbide epitaxial growth reactor and gas manifold diagram. 16

Figure 2.2: Image of the CVD system used for epitaxial growth of SiC, a) Close-up of CVD reactor during epitaxial growth; b) Over view of entire CVD system. 17

Figure 2.3: Visual of the resistive graphite heating element during epitaxial growth at 1650 ˚C, the 4H-SiC substrate can be seen in the middle with two 6H-SiC insulating pieces on either side for positioning. 18

Figure 2.4: Depiction of a probe in contact mode for AFM microscopy. 21

Figure 2.5: Depiction of SEM/EDS detection system. 22

Figure 2.6: Depiction of primary ion sources bombarding the multiwalled surface of the sample; charging can also be seen as the primary ions spread through the films. 23
Figure 3.1: Step bunching caused on on-axis 4H-SiC after in-situ hydrogen etching. The sample shown was etched for 15 minutes at 1700 ˚C; step heights are approximately 75 nm. 24
Figure 3.2: 4H-SiC on-axis average surface roughness, for 10 μm x 10 μm area after in-situ hydrogen etching and epitaxial growth. 25
Figure 3.3: SEM image of step-like surface features seen on on-axis 4H-SiC epitaxial growth, grown at 1650 ˚C with an approximate film thickness of 13 μm. 27
Figure 3.4: Cross-sectional SEM of C-face epitaxial film on on-axis 4H-SiC, ~14.83 μm±.05 μm. 29
Figure 3.5: Effect of temperature on deposition rate using on-axis 4H-SiC with an MTS molar fraction of 0.05%. 30
Figure 3.6: SEM images, magnified 500x, of on-axis 4H-SiC (Si polarity) epitaxial layers grown with 1 slm H_2, 4 sccm MTS. 31
Figure 3.7: Effect of MTS mole fraction and total flow rate on the deposition rate using on-axis 4H-SiC substrate at a growth temperature of 1650ºC. 33
Figure 3.8: Comparison of 4H-SiC on-axis and 8º off-axis epitaxial growth rates to that reported by Pedersen, *et al (2007)*. 34
Figure 3.9: SEM images of 4H-SiC epitaxial films grown at 1650ºC with a H_2/Ar of 0.1; Left: on-axis substrates, Right: 8º off-axis; MTS mole percents Top: ~0.025%, Middle: ~0.05%, Bottom: 0.09%, all images are displayed at 500X. 35
Figure 3.10: Stacking faults formed during 4H-SiC on-axis epitaxial growth; a) vertical and horizontal stacking faults, b) "step bunching" stacking faults. 38
Figure 3.11: Etch pits reviled after etching in potassium hydroxide, showing epitaxial growth of the same epitaxial film at different magnifications and regions; A: substrate, B: Epitaxial growth and C: Completely fill MPs. 39
Figure 3.12: SEM images of on-axis epitaxial growth that resulted in the presence of silicon droplets and homogenous 4H-SiC epitaxy on on-axis 4H-SiC (all images from same sample); a) after epitaxial growth, b) after HNA etch, c) after KOH etch, d)Threading edge dislocation (5k magnification). 40

Figure 3.13: On-axis 4H-SiC epitaxial growth at 0.05% MTS, 2 slm H_2 and 1500 °C, causing the formation of 3C-SiC. 41

Figure 3.14: Optical micrograph of 4H- on-axis SiC with graphite deposition on silicon polarity, due to an increased C/Si ratio of 3, magnification was 20X. 42

Figure 3.15: SEM images of 4H-SiC 4º off-axis SiC epitaxial layer and growth defects, with H_2:Ar of 1:1; a) and c) C/Si = 2, b) C/Si = 3. 43

Figure 3.16: a) Photoluminescence micrograph of cone-shaped defect and surrounding area showing TDs in red; b) Reflected white light optimal micrograph of cone-shaped defect; c) Micro Raman spectral analysis of defect and surrounding region, distinguishing between 3C-SiC and 4H-SiC polytypes. 44

List of Tables

Table 1-1: Electrical properties for three polytypes of SiC and other semiconductors, near room temperature.[9-14] 5

Table 1-2: Physical properties for three common polytypes of SiC and other semiconductors near room temperature.[16-20] 6

Table 1-3: Summary of high temperature/ power/ frequency applications for SiC.[21] 7

Table 3-1: Summary of test results obtained for the impurities of nitrogen, boron and aluminum [atoms/cm^3] in two epitaxial films grown at 1650 °C, 3.55 slm Ar, 350 sccm H_2, and 2.25 sccm MTS (0.05%). 36

Acknowledgements

I would first like to thank my major professor Dr. James Edgar for introducing me to material science and giving me the opportunity to pursue a higher degree in chemical engineering. I would further like to thank him for his support, guidance and instruction throughout my graduate studies.

I would also like to thank Dr. Douglas McGregor's group along with Jeff Blackwell, Laboratory manager for Nuclear Engineering for use of the scanning electron microscope, electron evaporator and wafer dicing saw. Additional thanks to Dr. Vikas Berry for supplying the atomic force microscopy equipment.

Immense appreciation goes to Office of Naval Research for their financial support, Dow Corning for supplying 6H-SiC wafers, and finally the Naval Research Laboratory and Evans Analytical Group for their assistance in characterizing of materials.

Additionally I would like to thank the help of my colleagues Dr. Peng Lu, Li Du, Yi Zhang and Clint Whitely for their support and help. Special thanks, is given to Dr. Peng Lu for helping me get started and sharing invaluable knowledge with me.

Final and most sincere thanks to my family and wife for unconditional support and encouragement.

Dedication

I dedicate this paper to my wife and family for all their loving support.

CHAPTER 1 - The Need for Something New

There are many types of semiconducting materials being used for modern electronic devices. However, many traditional semiconductors (Si, GaAs, Ge) are reaching their practical limit for many electronic applications. For example the maximum switching speed of silicon devices is 3 GHz, which is being used in modern computers. Many new applications in the military (equipment and vehicles), space (equipment and exploration), and automobiles are being developed for systems that will perform at high temperature, high frequency, and high power conditions. In general, the goal is to reduce system size and complexity, by reducing the size and amount of required cooling. What is needed is a semiconductor that can be easily incorporated into systems and circuits giving enhanced electrical and physical properties. Silicon carbide, SiC, is one such semiconductor, as it has better electrical and physical properties than silicon for certain types of electronics. SiC's wide band gap, coupled with the high break down field, high thermal conductivity, and high electron mobility has made it an excellent candidate for high temperature and high power electronic device applications.

1.1 Structure and Polytypes

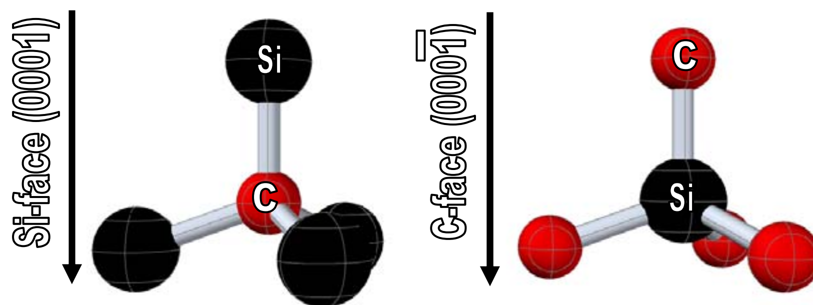

Figure 1.1: Tetrahedral bonding of carbon and silicon atoms in SiC, unit structure can consist as CSi_4 or SiC_4.

Prior to SiC's fame in the research world as a semiconductor, it was a rare natural gem, moissanite, found in iron-nickel meteorites (diamond quality) and man-made material used for sand paper and saw blades, due to its hardness. It is the only stable compound composed of only carbon and silicon and is tetrahedrally bonded as both CSi_4 and SiC_4,[1] as shown in Figure 1.1.

The carbon- silicon bonds are very strong, being 88% covalent and 12% ionic, with a bond length of approximately 1.89 Å. The distance between the second nearest neighbor is 3.08 Å.

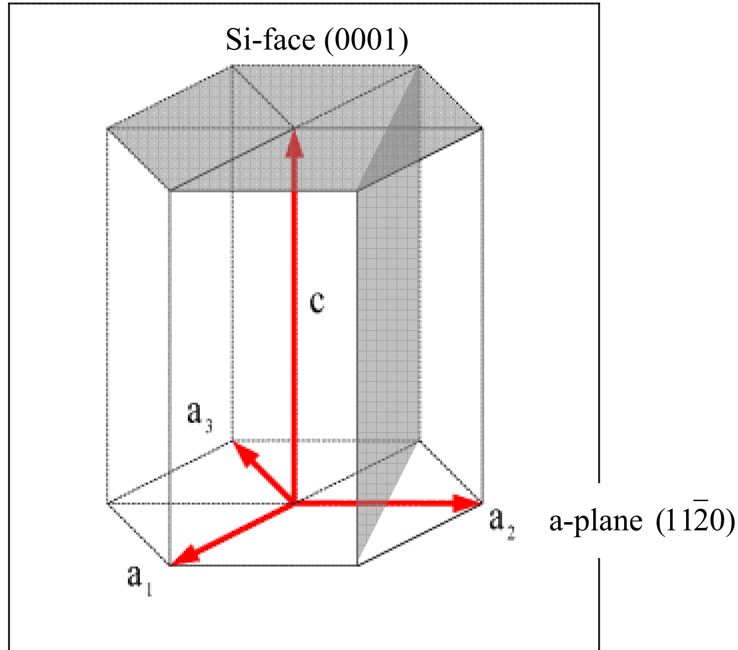

Figure 1.2: Hexagonal structure of a unit cell for 4H-SiC and 6H-SiC.

Similar to other biatomic semiconductors, hexagonal SiC has two distinct polar faces, Si-face (0001) and the C-face $(000\bar{1})$, and several non-polar faces, the most common of which are a-plane $(11\bar{2}0)$ and m-plane $(1\bar{1}00)$, as shown in Figure 1.2. Polarities are determined by the direction of growth and by the surface containing the highest surface concentration of either silicon or carbon, as shown in Figure 1.1. There are very distinct advantages and disadvantages between each plane. For instance, micropipes (MPs), large hollow core Burger vector screw dislocations that propagate in the c directional plane, can be eliminated when growing on non-polar surfaces.[3,4] However, non-polar face are not defect free; they contain higher concentrations of stacking faults and mis-alignments in stacking sequence (SFD).

One of the unique characteristics of SiC is its ability to form polytypes, a large number of different structures that have minor variations in stacking. All SiC crystal structures have three possible, two-dimensional, stacking planes in which biatomic, single silicon-carbon bond, molecules can organize. Figure 1.3 shows the three possible stacking overlays as A, B and C. Each variation in stacking sequence represents a different polytype of silicon carbide. By varying the number of layers and the sequence of layers, a large number of polytypes are

possible, reportedly over 250.[31] However, only two polytypes, 4H-SiC and 6H-SiC, are commercially available as wafers and therefore, are the focus of the vast majority of research for use in high power, high frequency and high temperature devices.

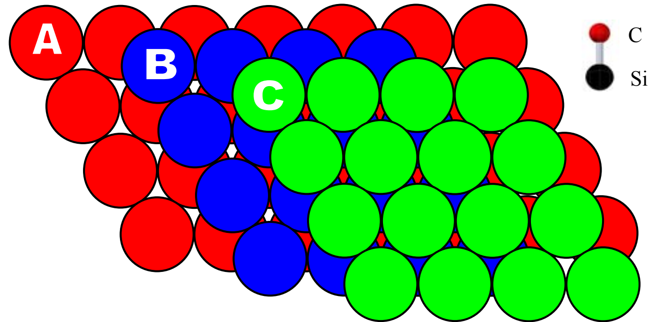

Figure 1.3: Possible stacking sequence locations in a close-packed crystal structure, perpendicular to the c-axis [0001]; the top right corner shows a carbon-silicon biatomic molecule.

The uniqueness of SiC is not only shown in its ability to form different polytypes, but that each polytype has distinctly different properties for high temperature, high frequency and high power applications. Many compounds exhibit a range of compositions, that deviate from ideal stoichiometry, but the Si:C ratio in silicon carbide, regardless of its polytype, is 1:1. For example boron carbide forms a 10.5:1 and 4:1 (B:C) ratio, instead of polytypes. However, each studied polytype has some similar and different properties. One such difference is the unit cell aspect ratios of the hexagonal polytypes, c/a, which is 3.271 for 4H-SiC and 4.098 for 6H-SiC respectively.[5]

The common nomenclature used for identifying the various polytypes of SiC is the Ramsdell notation. The Ramsdell notation, uses a number to signify the number of biatomic layers in each unique sequence before it is repeated and then is followed by a letter describing the polytypes symmetry, C – cubic, H – hexagonal and R - rhombahedral. Thus, 3C-SiC has a stacking sequence of ABC and a cubic (zinc blend) geometry. 4H-SiC and 6H-SiC have stacking sequences of ABCB and ABCACB, with a hexagonal geometry. Figure 1.4 shows stacking of biatomic layers for 3C-SiC, 4H-SiC and 6H-SiC.

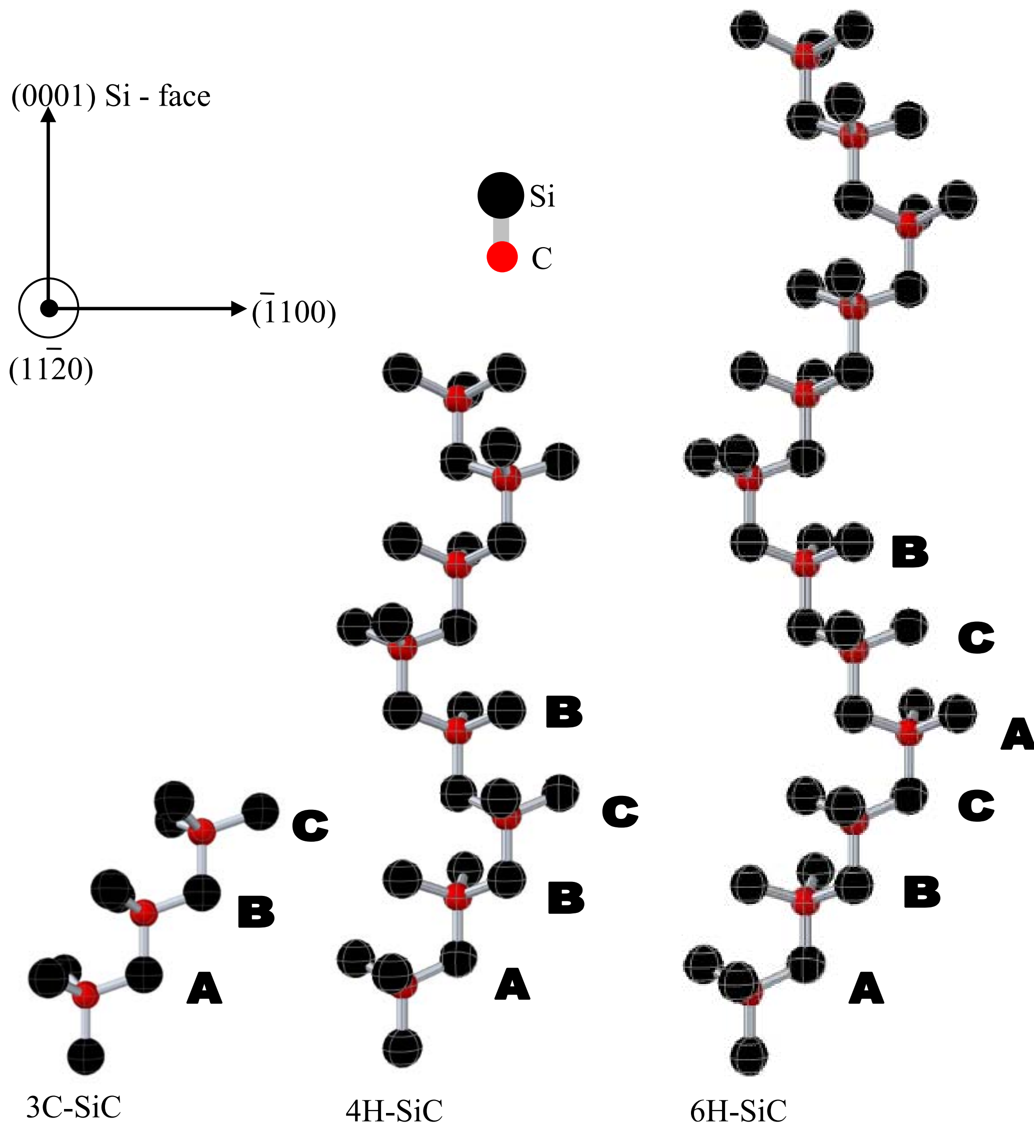

Figure 1.4: 3-D view of stacking sequence for 3C-SiC, 4H-SiC and 6H-SiC.

1.2 Electrical and Physical Properties

SiC's outstanding physical and electrical properties make it an excellent candidate for high temperature, high power and high frequency electronic devices. It is also amongst the strongest of materials, ranking at least a 9 on Mohs scale of hardness (diamond = 10).[6] In addition it is highly resistant to chemical reactions; it is not chemically etched by any acids or bases near room temperature. SiC's high operating temperatures, 300 – 600 °C, are due to its wide bandgap. These properties make SiC an excellent candidate for electronic devices operating in harsh environments, such as other planets.

1.2.1 Electrical Properties

Table 1-1: Electrical properties for three polytypes of SiC and other semiconductors, near room temperature.[9-14]

Electrical Properties	Semiconductor					Ref
	3C-SiC	4H-SiC	6H-SiC	Si	GaAs	
Band Gap [eV] Liquid N_2	2.39	3.26	3.02	1.1	1.4	9, 10
Indirect (I)/Direct (D) Band Gap	I	I	I	I	D	10
Mobilities [$cm^2/V{\cdot}s$] @ 300K						
Electrons	1000	800	400	1500	8500	9
Holes	40	140	101	450	400	
Breakdown Field [10^6 V/cm]	2.1	2.2	2.4	~0.3	~0.4	11
Drift Velocity [10^7 cm/s]	2.0	2.0	2.0	1.0	2.0	12
Electrical Resistivity [$\Omega{\cdot}cm$]		10^2 - 10^6		10^{-3} - 10^4		13,14

SiC has many advantageous electrical properties for high power, high frequency devices in comparison to conventional semiconductors, like silicon and gallium arsenide. The wide band gap of 4H-SiC, 3.26 eV, is approximately 3X that of silicon, 1.16 eV. It has a high maximum switching frequency, response speed of on- and off-switches like transistors, of 10 – 100 GHz, which towers over silicon's 3 GHz capability.[7] Other properties, such as increased power density and very low current leakage will improve response time, speed and reliability of electronic devices. Thus SiC devices may out perform silicon based devices at one-fortieth the size.[8] Though it is efficient for high power applications, it is inefficient for optoelectronics, LEDs, and laser diodes because of its indirect band gap.

1.2.2 Physical Properties

Table 1-2: Physical properties for three common polytypes of SiC and other semiconductors near room temperature.[16-20]

Physical Properties	Semiconductor					Ref
	3C-SiC	4H-SiC	6H-SiC	Si	GaAs	
Lattice Geometry	Zincblend (cubic)	Hexagonal	Hexagonal	Diamond	Zincblend	
Lattice Constant [Å] @ 300K						
a =	4.3596	3.073	10.053	5.4305	5.6533	11,12
c =		3.073	15.118			
Density [g/cm^3] @ 300K	3.166	3.21	3.211	2.328	5.32	15,16
Thermal Conductivity [W/cm·K]	3.2	3.7	3.6	1.5	0.46	15
Refractive Index (ordinary array)						
λ = 498nm	2.6916	2.698	2.6894			15
λ = 467nm	2.5538	2.561				17
IR Refractive Index @ 300K						
⊥c	2.55	2.55	2.55	3.42	3.3	11
"if applicable" ∥c		2.59	2.59			
Linear Expansion Coefficient (10^{-6} K^{-1})	3.9		4.46 a-axis 4.16 c-axis	2.6	6.86	19
Heat Capacity [J/g·K]	0.71			0.7	0.33	15
Mohs Scale for Hardness	9.2 - 9.3			7	~4.5	16
Melting Point [˚C]	2730	2730	2730	1415	1238	

Electrical properties are not the only advantages that make SiC such an impressive semiconductor, its physical properties are also of interest to researchers and manufacturers. The high thermal conductivity, 3.2 – 3.7 W/cm·K, coupled with the wide bandgap gives SiC based devices an advantage, by increasing the maximum operating temperature from 300 ˚C to 600 ˚C, [15] approximately 3X greater than many current devices. Additionally, SiC has the ability to rapidly disperse heat due to its high thermal conductivity, 3.2 W/cm·K, which is similar to that of copper, 4.01 W/cm·K. These properties will decrease the need for costly cooling systems and the overall weight of the equipment (i.e. complete removal of cooling fans).

1.3 Applications

4H-SiC and 6H-SiC are commercially available semiconductors with great potential for high temperature, high power and high frequency electronic devices. There are a wide variety of applications for SiC devices in the military, space program, automobiles and more. It is also a frequently employed substrate for optoelectronic devices, such as blue and green LEDs and laser diodes, that use GaN epitaxial layers.

Table 1-3: Summary of high temperature/ power/ frequency applications for SiC.[21]

Industry	**Devices**	**Key Advantages**
Automobile	High temp sensors, High power integrated systems	Higher efficiency (low leakage), Direct internal engine monitor
Military, Spacecraft	Transistors, Diodes, High temp/inert sensors	Reduction of radiant cooling, Radiation resistance
Power	High power/temperature "smart" devices	Increase response time, decrease in cooling systems,

1.4 Growth Chemistry

SiC crystals can be grown as single crystal boules and epitaxial layers. For single crystal boule growth, physical vapor deposition, also know as sublimation, is used. This differs from boule growth of many semiconductors, such as silicon which uses liquid melt growth, because of the excessively high melting point of SiC, 2783 ˚C. Sublimation produces single crystal boules which can be sliced into wafers for use as substrates, Figure 1.5A. On the other hand epitaxial thin films, <200 μm, produced by chemical vapor deposition, are used for fabricating devices, Figure 1.5B. Chemical vapor deposition, CVD, gives the operator the ability to control the conditions, growth rate, and electrical properties of the thin films. The ability for the operator to control most aspects of CVD can result in high quality and high purity materials.

Figure 1.5: A) 4H-SiC single crystal boule produced using the modified Lely process; B) Epitaxial layer grown on 4H-SiC with a thickness of ~5 μm.

1.4.1 Bulk Crystal Growth

In 1955 Lely developed the first process for growing high quality single crystals of 6H-SiC, known as the Lely process.[22] The Lely process used polycrystalline SiC, which were packed between a porous graphite cylinder and graphite crucible, schematically shown in Figure 1.6. The graphite crucible was then covered with a graphite lid and heated to approximately 2500 ˚C in atmospheric argon, well above the sublimation conditions. The chamber quickly filled with vapors, most commonly Si, Si_2C and SiC_2, which would deposit on the lid, base and SiC source clusters (as platelets). The process was capable of producing very high quality SiC;

however the yield was very low and incapable of controlling size, shape, and polytype of the crystals.[23]

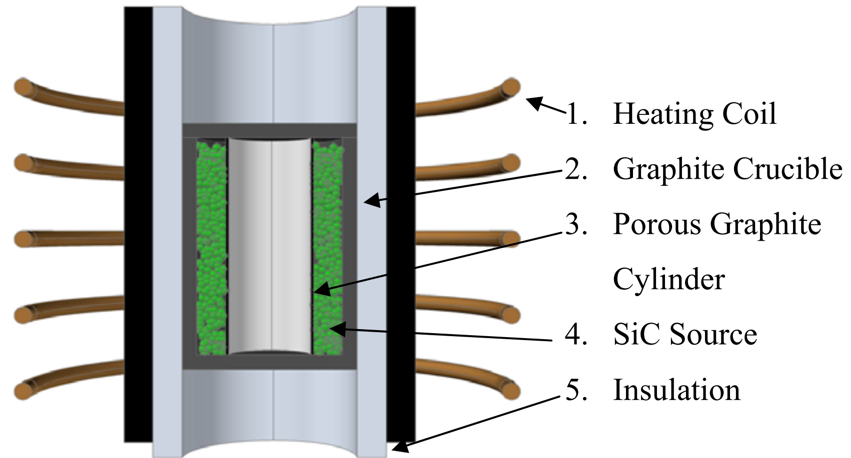

Figure 1.6: Basic diagram of Lely's reactor setup.

Then in 1978 Tairov and Tsvetkov modified the Lely process by using a seed crystal to orient the growth direction and polytype. The SiC source, either as a powder or as polycrystalline SiC, was packed in the base of the crucible and the seed crystal was attached to the lid, shown in Figure 1.7. The temperature was decreased to approximately 2200 ºC, and the pressure reduced below atmosphere, still using argon. A temperature difference between source and the seed of approximately 20 ºC was imposed to enhance the growth rate. The temperature difference forced the sublimed source to migrate toward the cooler seed, where it would condense causing crystal growth. This process was so successful that in 1987 students from North Carolina began Cree Research Inc., a company dedicated to SiC based products. By 1990 Cree had commercialized 25 mm single crystal wafers.[24] Over the years more companies have begun producing 4H-SiC and 6H-SiC, with commercially available wafers reaching 4in in diameter. Though wafers are commercially available and contain electrical properties suitable for devices, they have high defect densities that limit their use and degrade the device performance. Epitaxial growth also suffers from the high defect densities, near 100 cm^{-2}, which may propagate through the epitaxial films.

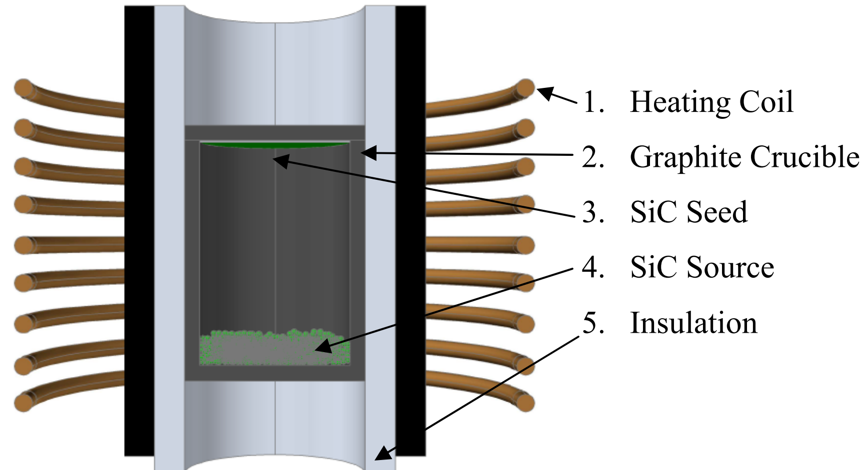

Figure 1.7: Basic diagram of modified Lely process.

Additional improvements to the Lely process have led to companies, such as Cree, Dow Corning and Northrop Grumman, to release larger diameter and micropipe free 4H-SiC and 6H-SiC wafers. These modifications were first introduced by Toyota Central R&D and DENSO Corp, in which a two step process was used.[25] This process is very similar to the pervious modified Lely process in that it uses a seed crystal; however in this two step method, the seed crystal is grown on the a-axis first, labeled "new growth" in Figure 1.8, to eliminate micropipe defects. Though this makes the crystal micropipe free, the growth along the a-axis produces a high concentration of stacking faults, as mentioned previously. Therefore, the "new growth" is sliced along the c-axis, where it may growth free of micropipes and reduce the number of stacking faults.

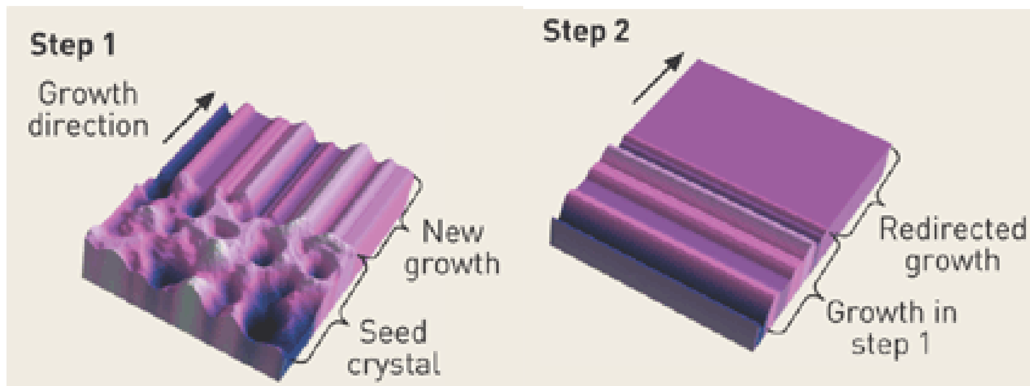

Figure 1.8: Two step method proposed by Toyota Central R&D and DENSO Corp., to produce micropipe free SiC.[25]

1.4.2 Epitaxial Growth

Homoepitaxial growth is thin film growth on the surface of a substrate, in which the film is single crystal and oriented in the same direction of the substrate. The most common method for epitaxial growth is chemical vapor deposition, CVD. In CVD gas phase reactants enter the reactor and decompose into radicals that migrate to the surface of a substrate where they react with each other and the substrate to deposit as a solid thin film. Nucleation is typically favored at steps, crevices or defects on the surface of the substrate, because these sites have the lowest potential, allowing the nucleated species to attain minimum energy. However, at high saturations nucleation can occur on flat regions and terraces where the potential is high. For SiC, terrace growth is typically undesired because it has the disadvantage of promoting growth of multiple polytypes.

The two most common types of CVD reactors for thin film epitaxial growth are hot and cold walled (water cooled) reactors, typically operated at low pressure, LP, or ultrahigh vacuum, UHV, to help prevent undesired side reactions. The major differences between hot wall and cold wall CVD are the source reactants used and the uniformity of heating. For instance, solid or powder-type sources be used to react with gases or vapors to create a volatile reactant; such as hydrogen chloride reacting with gallium to form gallium chloride for use in gallium arsenide and gallium nitride epitaxy. On the other hand a cold wall CVD reactor can't use solid type materials as they would condense on the reactor walls, but is ideal for metal organic CVD (MOCVD), which deposits on all hot regions. Another major difference is the heating of the substrate, which can be more uniform with hot wall CVD. This is because the resistive heating element surrounds entire substrate, heating both the source and substrate simultaneously, where in the cold wall reactor the resistive heating element heats the substrate directly. Though it is possible to have uniform heating of the substrate in cold wall CVD, there are very large temperature gradients at small distances from the substrate that can't always be controlled, which may cause deposition on many surfaces.

Typically, 4H-SiC and 6H-SiC epitaxy by CVD uses silane (SiH_4) with a hydrocarbon source, such as propane (C_3H_8), in a cold wall reactor. Three moles of silane and one mol of propane will produce three moles of SiC, as shown in equation 1.1. However, the deposition rate of this method is dependent on the homogenous decomposition of silane to silicon, as shown in equation 1.2, which can limited the growth rate to an average of 10 μm/hr and deposit silicon

droplets on the surface. Consequently, deposition of uniform films greater than 150 μm is not cost effective due to the extensive reaction times required at such low growth rates. Other disadvantages of silane and propane precursors are the environmental, health and storage hazards. Storage poses a problem because the compounds are gaseous at room temperature and therefore harder to contain. Major hazards associated with silane are the toxicity, at 5ppm, and pyrophoricity with an auto ignition temperature less than 85 ˚C. Propane is a more stable compound, but still poses a hazard as a combustible gas.

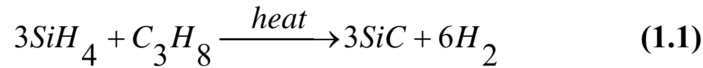

$$3SiH_4 + C_3H_8 \xrightarrow{heat} 3SiC + 6H_2 \qquad \textbf{(1.1)}$$

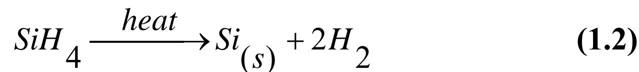

$$SiH_4 \xrightarrow{heat} Si_{(s)} + 2H_2 \qquad \textbf{(1.2)}$$

The uses of methyltrichlorosilane, MTS, for producing SiC are not new; it was primarily used to deposit polycrystalline SiC on graphite as a protective coating.[26] In early work, Gorin *et al.* reported it could be used for bulk single crystal growth of 3C-SiC on an unseeded graphite scepter. They reported the growth of high quality crystal at approximately 500 μm/hr, producing crystal near 3 mm x 1.5 mm x 5 mm.[30] MTS has more recently been chosen as a single precursor for SiC epitaxy because it is an all-in-one source, liquid at room temperature, and inherently safer than silane and propane. It has an added advantage of containing chlorine, which can improve epitaxial growth. The disadvantage of MTS is its fixed ratios of Cl/Si = 3, and Si/C = 1. Optimized growth may require independent control of these ratios.

The thermal decomposition of MTS at temperatures above 1400 K occurs via equations 1.3 and 1.4. Though there are near 100 different possible side reactions when decomposing MTS thermally in the presence of hydrogen at temperatures above 1400 K, the formation of trichlorosilane and methyl radicals are the most thermodynamically plausible, as shown by Yingbin.[27] Thus, at the surface of the substrate, nucleation occurs causing the formation of SiC and hydrogen chloride.

$$CH_3SiCl_3 \xrightarrow{1400K} SiCl_3^* + CH_3^* \qquad \textbf{(1.3)}$$

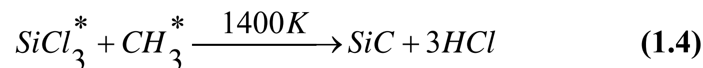

$$SiCl_3^* + CH_3^* \xrightarrow{1400K} SiC + 3HCl \qquad \textbf{(1.4)}$$

The presence of chlorine during decomposition and nucleation is believed to suppress unwanted terrace growth, decrease gas phase nucleation of SiC, and reduce the formation of

silicon droplets on the surface. This makes it possible to greatly increase the quality and rate of growth. By decreasing gas phase nucleation (the formation of crystals in the gas phase), nucleation will occur primarily at the surface of the substrate, so the growth rate can be increased to >100µm/hr and the crystal quality improved by keeping the crystals formed in the gas phase from reaching the surface. Suppressing terrace growth and reducing the formation of silicon droplets improves the quality of the films, by reducing the presence of multiple polytypes, mainly 3C-SiC, and reducing variations in growth rates along the surface.

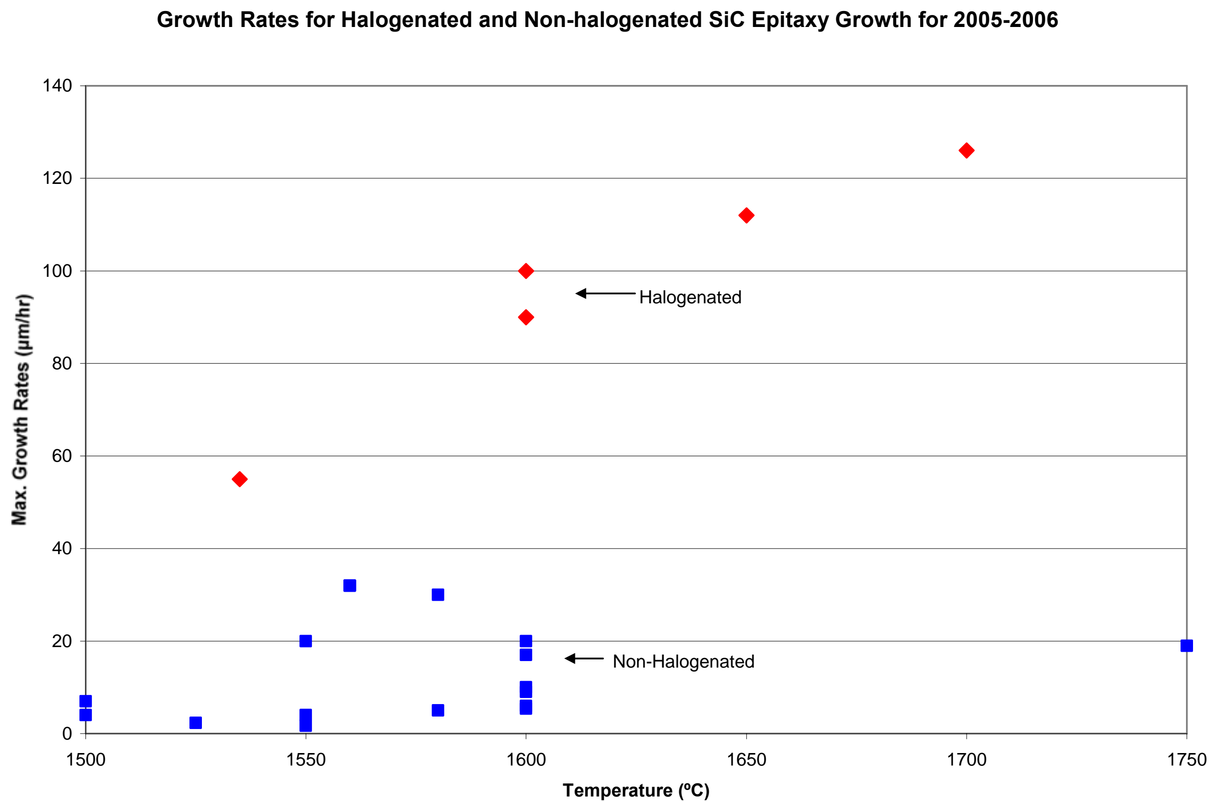

Figure 1.9: Maximum growth rates from multiple references, dating 2005 – 2006, achieved using non-halogenated and halogenated precursors.

The choice of substrate orientation, degrees/angle cut from the c-plane, can have major impact on the cost of wafers, the surface quality and propagation of defects in the SiC films. More on-axis than off-axis wafers can be sliced from a single crystal boule, reducing the amount of high quality single crystalline waste. Epitaxial film quality as judged by defect density can also be greatly impacted by the orientation of the substrate. Epitaxial films grown on on-axis substrates can convert nearly all micropipes and basal plane dislocations, which are detrimental

to devices, into threading edge and screw dislocations,[28] whereas on large misorientations, tilted 3º - 8º toward a-axis, substrate defects are propagated into the epitaxial layer[29]. However, off-axis orientations have an advantage of replicating the substrate polytype into the epitaxial layer by the "step growth" method. 3C-SiC inclusions may also be reduced due to a decrease in terrace size on the surface of the substrate, as shown in Figure 1.10. The larger the degree of misorientation, the higher the step density, which as mentioned previously has a low potential and therefore can promote growth. However, due to the cost effectiveness and capability of reducing defects with on-axis substrates, it is the main focus of this research.

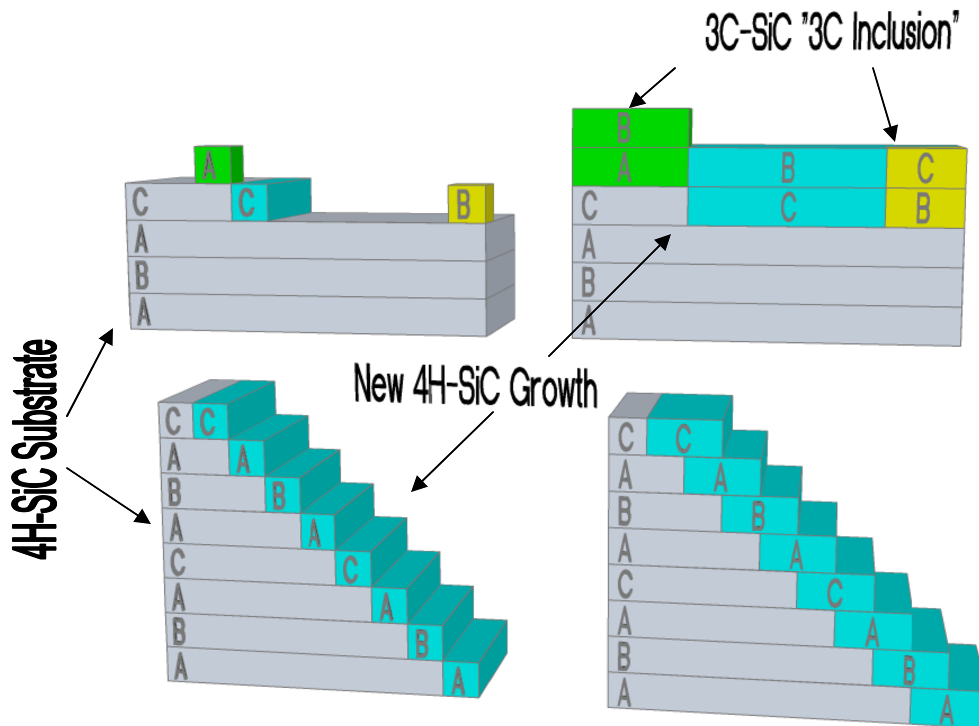

Figure 1.10: Step growth mechanism shown on 4H-SiC, (Top) Vertical growth on an on-axis substrate, showing 3C-SiC inclusions (ordering CAB and ABC), (Bottom) 4H-SiC step growth on a large off-axis angled substrate, parallel to substrate steps produces the same polytype as the substrate.

Temperature also greatly affects the quality, growth rate, and polytype of the epitaxial film. Deposition of the 3C-SiC polytype is a common when using low temperatures from 1300 – 1500 ˚C, regardless of the substrate polytype. This is due to the low surface mobility which prevents the reactants from reaching the step edges. Therefore, growth temperatures for 4H-SiC and 6H-SiC epitaxy typically range from 1500 – 1800 ˚C, because temperatures above 1600 ˚C

make the 3C-SiC polytype unstable and shift the equilibrium toward 4H-SiC and 6H-SiC.[30] The temperature also controls the maximum growth rate of the epitaxial film, as shown in Figure 1.9. Though higher growth rates can be achieved at higher temperatures, the quality of the film, for temperatures >1750 ºC, degrades toward producing polycrystalline SiC.[31]

Early reports for SiC epitaxy with MTS used 6H-SiC substrates. Zelenin *et al,*[32] used MTS to grow 6H-SiC on on-axis 6H-SiC (0001) substrates. They reported that the precursor was capable of producing 6H-SiC, but the film had many 3C-SiC inclusions and stacking faults, as is typical of on-axis epitaxial growth. More recent reports for MTS epitaxial growth on off-axis, tilted >4˚ toward a-axis, 4H-SiC and 6H-SiC substrates produced higher quality films, without the presence of 3C-SiC inclusions, lower defect densities (<50 cm^{-2}), and high growth rates (>100 μm/hr).[31] MTS has also shown capable of producing epitaxial layers thicker than 200 μm with near uniform thickness.[31,35] Thus, MTS is a suitable precursor for a wide variety of devices.

Though MTS has proven capable of good quality and high growth rates of SiC epitaxy, the fixed C/Si and Cl/Si ratios of 1/1 and 3/1 may limit the ultimate quality of SiC epitaxial films. These ratios affect the unintentional impurity concentrations, the incorporation of additional elements altering the electrical properties of SiC epitaxial layers. However, the effects of chlorine have not been extensively studied. Thus, understanding of how each reactant ratio affects such parameters is needed. Pedersen *et al.*[35] did extensive studies in altering these ratios with the addition of propane and silane to determine the affect of the C/Si ratio on the growth rate and impurity incorporation of off-axis epitaxial films. All the experiments were done on the Si-face (0001), using 8˚ off-axis 4H-SiC, with a fixed Cl/Si ratio of 3 except when adding silane. Both the Cl/Si and C/Si ratios directly affected the growth rate with the highest achievable growth rate, >100μm/hr, when Cl/Si = 3 and C/Si ≥ 1. Decreasing either ratio decreased the growth rate proportionally. The net impurity concentrations were directly dependent on growth rate and C/Si ratio, such that the minimum net concentration of 10^{14} cm^{-3} was achieve at a C/Si = 1 which is similar to other values reported when using silane and propane precursors[33,34]. Pedersen *et al.*[35] found that the nitrogen incorporation, the most common element employed for n-type doping, increased for growth rates <75 μm/hr and C/Si <1. Aluminum, p-type doping, was just the opposite and increased when growth rates > 75μm/hr and C/Si >1.[35] Thus, the affect of doping and C/Si ratio agrees with Larkin's "site-competition theory", in which nitrogen replaces carbon and aluminum replaces silicon.[36]

CHAPTER 2 - Experimental

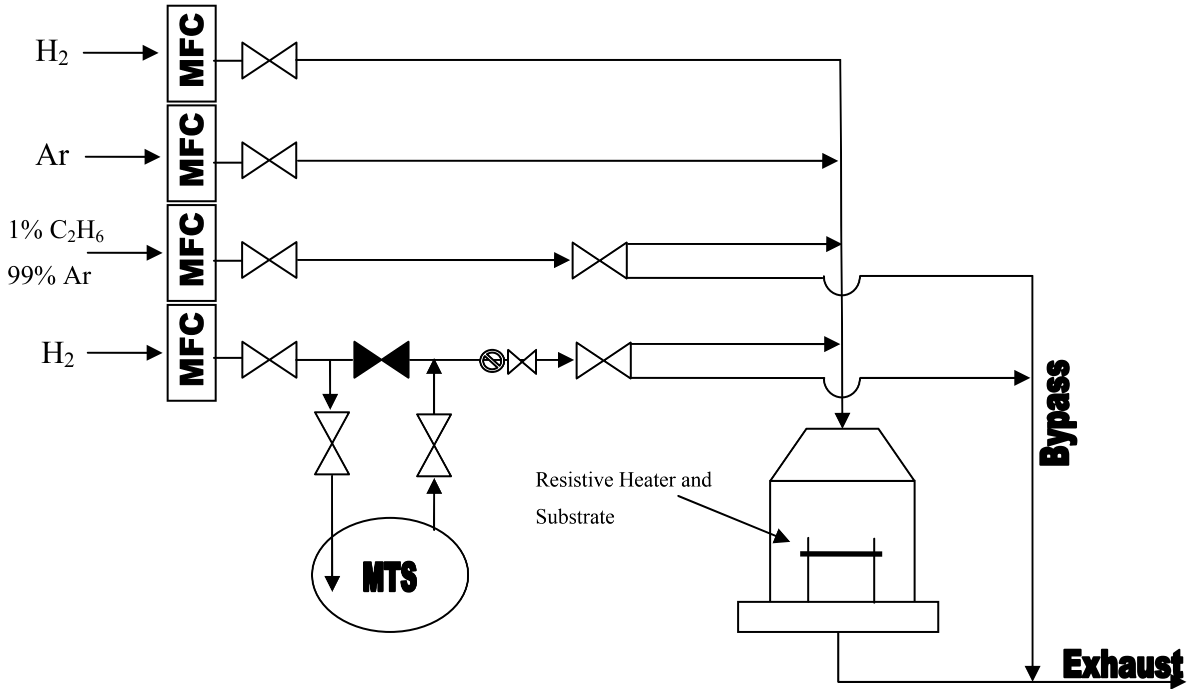

Figure 2.1: Silicon carbide epitaxial growth reactor and gas manifold diagram.

The main focus of this paper is the epitaxial growth of 4H-SiC on on-axis 4H-SiC substrates. For homoepitaxy, there are many benefits to using on-axis substrates, such as their lower cost and the ability to convert micropipes and stacking faults into threading edge dislocations during epitaxial growth. Unlike off-axis growth, on-axis growth is not capable of "step growth", thus homoepitaxial growth presents a difficulty due to increase potential of producing 3C-SiC inclusions. The use of a chlorinated precursor may reduce the density of 3C-SiC inclusions on off-axis substrates by etching the surface during growth and decreasing gas phase nucleation. Therefore, experiments were performed to produce 3C-SiC free SiC epitaxial films on on-axis silicon carbide, with a minimum growth rate of 10 μm/hr.

2.1 Reactor and Heating Element

For all deposition experiments, a custom made vertical cold wall CVD reactor was used. The main components of this system consisted of a vertical quartz reactor, resistive graphite heating element, a gas manifold apparatus, pyrex bubbler (containing methyltrichlorosilane), vacuum/ pressure control system and a control consol, as seen in Figure 2.1 and Figure 2.2.

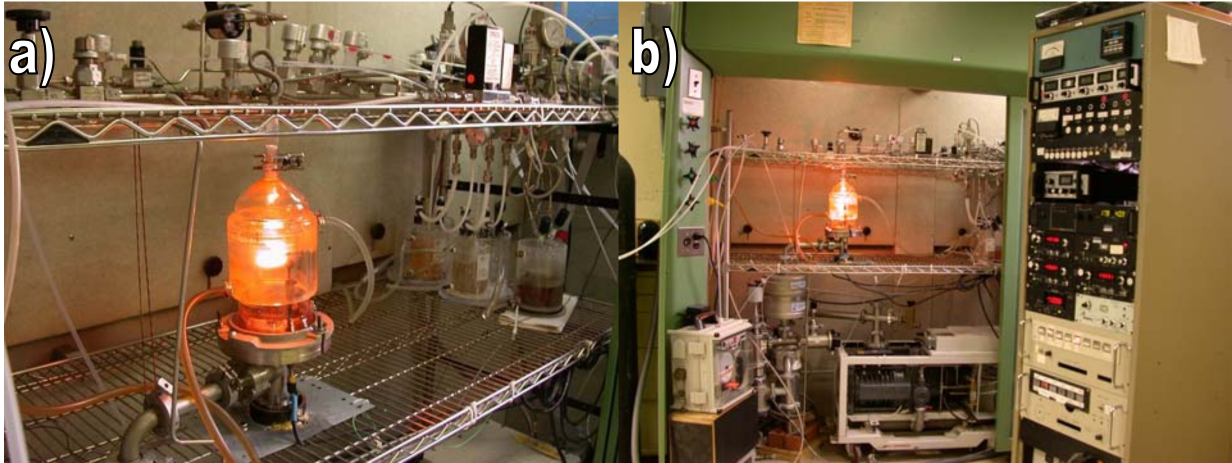

Figure 2.2: Image of the CVD system used for epitaxial growth of SiC, a) Close-up of CVD reactor during epitaxial growth; b) Over view of entire CVD system.

The power (hence the temperature) to the resistive graphite heating element was controlled using a Sorensen DCS power supply. A previous design of the graphite heater, by Dr. Peng Lu, was used for its capability of reaching 1900 ºC and successful use in CVD epitaxy. However, two problems initially existed with the heating element design, such as the substrate easily falling off due to vibrations caused by the pumps and decomposition of the heating element by hydrogen etching at high temperatures. To prevent the substrate from falling off the heating element, a 15 mm x 12 mm x 1 mm volume was bored from the center to house the substrate, as seen in Figure 2.3. Etching of the heating element was reduced by coating the heating element, with a thin layer of polycrystalline SiC, prior to experimentation, using MTS at reaction conditions. Coating the heating element also helped regulate the C/Si ratio by suppressing the release of additional unknown amounts of carbon at high temperatures.

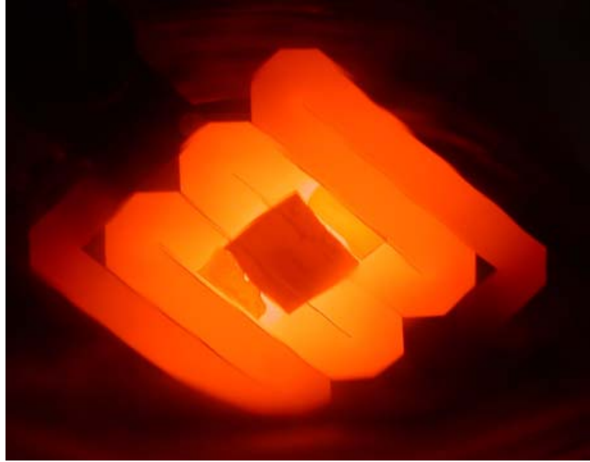

Figure 2.3: Visual of the resistive graphite heating element during epitaxial growth at 1650 ˚C, the 4H-SiC substrate can be seen in the middle with two 6H-SiC insulating pieces on either side for positioning.

2.2 In-situ Hydrogen Etching

Prior to SiC epitaxial growth, in-situ hydrogen etching was used to clean and remove polishing scratches from the surface. By removing the polishing scratches, the presence of 3C-SiC and uneven growth of the epitaxial film may be reduced. Reports have shown that the 4H-SiC surface begins to etch at temperatures over 1500 ˚C in the presence of hydrogen.[37,38] Off-axis substrates are usually etched to produce the smoothest surface, with regular step features, prior to epitaxial growth. However, etching on-axis substrates produces large triangular features known as “step bunching”, during the etching process. Therefore the purpose of these experiments was to determine the optimal conditions for etching on-axis 4H-SiC above atmospheric pressure, so subsequently smooth epitaxial films can be produced.

The substrates were prepared for hydrogen etching by dicing the wafers into 10 mm x 5 mm substrates and cleaning in trichloroethylene, acetone, methanol ultrasonic bath and water to remove organic oils and particles from the surface. Two substrates, one carbon face up and the other silicon face up, were loaded into the CVD reactor. The reactor was purged with hydrogen and evacuated for six hours to a base pressure of 10^{-5} torr. Hydrogen etching took place for ten minutes, at 800 torr and 2 slm (standard liters per minute) hydrogen, over a range of temperatures from 1400 ˚C to 1650 ˚C. After analysis of the surface using AFM, epitaxial growth was performed on each substrate, using identical conditions for direct comparison, and then analyzed with AFM to determine the optimal etched surface for epitaxial growth.

2.3 Epitaxial Growth

Methyltrichlorosilane was used as a single source precursor, except when experimenting with increase C/Si ratios, in which a 1% ethane in argon was used as well. The volumetric flow rate of MTS was controlled by saturating the hydrogen carrier gas with its vapors. To maintain a constant MTS flow rate, the bubbler was submerged in an ice bath to keep a constant vapor pressure of 50 torr. The bubbler pressure was also maintained at 500 torr, using a needle valve and automatic controller, allowing the saturation flow of MTS to be calculated by equation 2.1. Reactor pressure was maintained at 200 torr during the reaction phase, with temperatures ranging from 1600 °C to 1800 °C. All epitaxial layers were deposited for 60 minutes with a range of MTS mole flow rates from 17 mmol/min to 86 mmol/min.

$$V_{H_2} \cdot \frac{P_{vap}}{P_{bubbler}} = V_{MTS} \qquad \textbf{(2.1)}$$

Studies were done to compare the surface morphology and growth rates of 4H-SiC epitaxy on Si-face, on-axis and 8° off-axis substrates using low volumetric fractions of MTS, from 0.025% to 0.10%, with an H_2/Ar ratio of 0.2 and total gas flow rate of 4.5 slm. Additional studies were done to determine the effect of the H_2/Ar ratio, temperature and surface polarity on the growth rate and surface morphology of 4H-SiC on-axis and 4º off-axis substrates. Finally, the effect of an increased C/Si ratio, from 0.0 to 2.0 using additional ethane, on the presence of silicon droplets were studied.

2.4 Defect Selective Etching

Defect selective etching of SiC substrates and epitaxial films was done to identify defects in the samples, such as threading edge and screw dislocations, and to determine whether the defects propagate into the epitaxial films. For this, each substrate was submerged in molten potassium hydroxide at 500 ˚C contained in a platinum crucible. Each sample was etched for two minutes, which was the determined length of time capable of producing the desired effect at these conditions. Samples were subsequently examined by optical and electron microscopy to determine the pit shape, size and density.

Silicon was selectively removed by etching in a HNA solution, without etching the silicon carbide. This allowed for direct analysis of the epitaxial film and the origin of the silicon droplets. The HNA acid solution was a mixture of 27% acetic acid, 27% hydrofluoric acid and

46% nitric acid. Samples with solidified silicon droplets on the surface were etched at room temperature for 20 minutes to ensure that all silicon was etched away. Samples were examined by electron microscopy to ensure proper etching of silicon.

2.5 Characterization Techniques

The SiC epitaxial films were characterized by five different analytical techniques. These included optical microscopy, atomic force microscopy, scanning electron microscopy, energy dispersive spectroscopy, secondary ion mass spectroscopy and micro Raman spectroscopy. These techniques allowed the analysis of surface roughness, surface morphology, defects, growth rate and elemental concentrations.

2.5.1 Atomic Force Microscopy

Atomic force microscopy (AFM) analyzes the roughness of a surface and render a three dimensional image. The roughness analysis was determined by a Easyscope II and an analysis program provided by Dr. Vikas Berry of Kansas State University. Surface analysis with AFM was mainly employed in hydrogen etching experimentation to determine the optimal hydrogen etching conditions before SiC epitaxy. The surface roughness of the polished surfaces (as received by the manufacturer), post hydrogen etching, and post epitaxial growth were measured by AFM.

The instrumentation can analyze the roughness by either contact or non-contact (tapping) mode. Contact, also know as static or repulsive, mode was applied for all analysis in this paper as it is typically for hard flat surfaces that can't be damaged by the probe tip. AFM works by lightly scanning a probe tip or cantilever, typically measuring a couple of nanometers in diameter, over the surface with set contact force. Surface characteristics are measured by changes in the angle of the refracted laser due to repulsive force acting on the probe moving it toward or away from the surface, as show in Figure 2.4. The angle of the probe is measured using a focused laser, which refracts off the tip, and is detected by a photodiode.

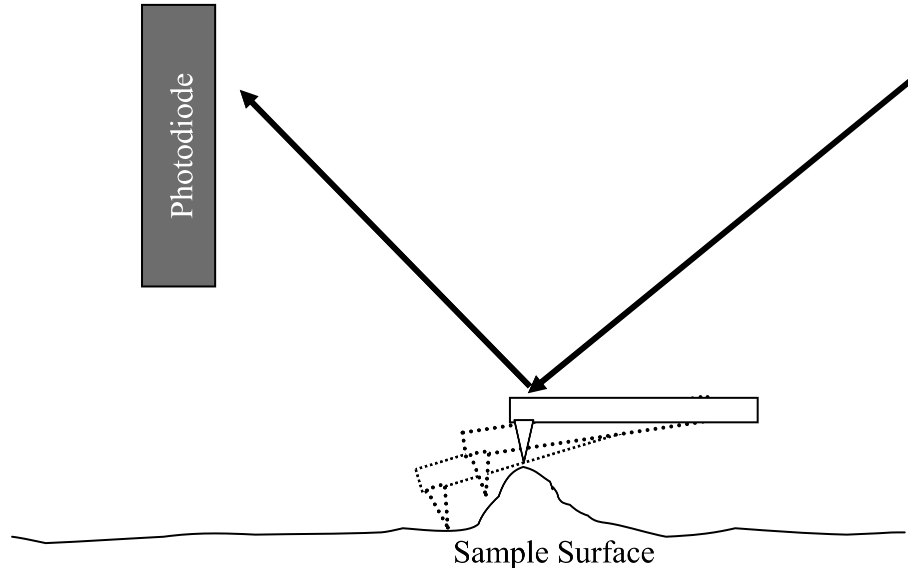

Figure 2.4: Depiction of a probe in contact mode for AFM microscopy.

2.5.2 Scanning Electron Microscopy/Energy dispersive spectroscopy

Scanning electron microscopy (SEM) is one of the most widely employed methods for surface characterization by the semiconductor industry. A Hitachi 4500-N SEM with an energy dispersive spectroscopy (EDS) attachment was provided by Dr. McGregor of Kansas State University. Surface morphology/defect characterization of the substrates and epitaxial films were done by SEM. Cleaved cross-sections of epitaxial films were examined to measure the film thickness for growth rate analysis. A qualitative mapping of concentrated silicon deposits on the surface of epitaxial films were made with EDS.

SEM works by bombarding the surface of the sample with a focused beam of electrons, which produces back scattered and secondary electrons. Secondary electrons are collected and analyzed by the detector to produce an image of the surface whereas the back scattered electrons are typically ignored but may be collected to help define the contrast of the surface. The quality of the image is highly dependent on the intensity of the secondary electrons detected. To increase the secondary electron output, thin conductive layers, ~1-3 nm thick, where sputter coated on the surface of samples. Therefore, prior to imaging many non-conductive surfaces, such as undoped SiC, are sputter coated with carbon or other conductive metals, ~few nanometers thick. Thin conductive layers were applied to samples in these experiments by a Hummer VI plasma sputter coater, containing a graphite source.

The elements of a sample were qualitatively measured with EDS. Typically attached to a SEM, EDS collects and analysis x-rays produced by electron beam contacting the surface, as shown in Figure 2.5. Since all elements produce unique x-ray wavelengths, the detector can analyses the signals to determine which atom they came from. By coupling EDS with SEM, a detailed map of elemental concentrations can be produced. Subsequently the map can be overlaid onto a corresponding SEM image, for better analysis of features. Similar to the SEM the intensity of the excited electrons is very important to get an accurate analysis of the sample.

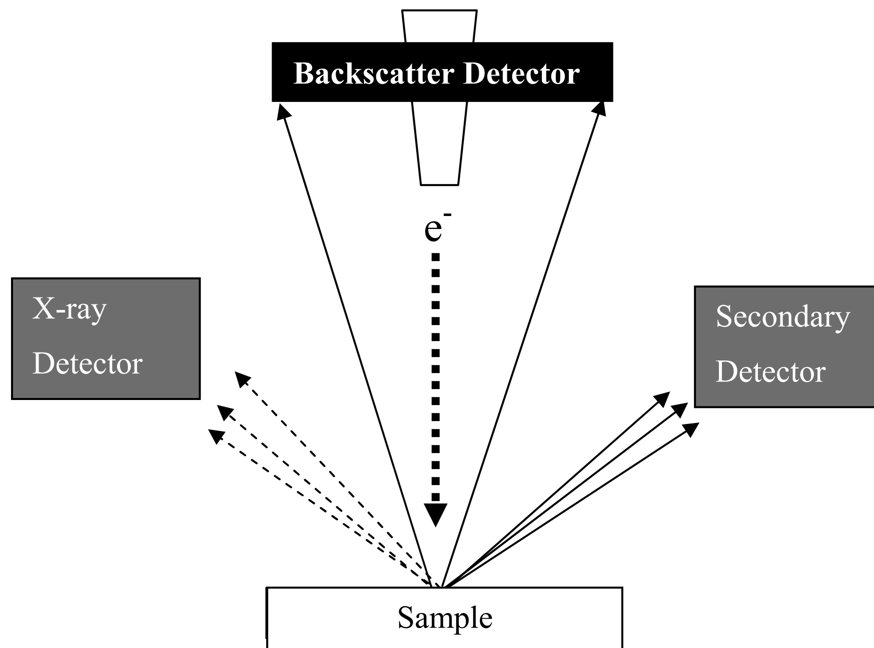

Figure 2.5: Depiction of SEM/EDS detection system.

2.5.3 Secondary Ion Mass Spectrometry

Secondary ion mass spectroscopy (SIMS) was performed by Evans Analytical group. Similar to EDS, SIMS is used as an analytical technique for elemental concentrations. However, unlike EDS, this technique is quantitative and very accurate. Unintentional doping impurities were quantitatively determined by this method. Boron, nitrogen and aluminum, the most common dopants, were measured within epitaxial films grown on both the Si- and C polarities using the same experimental conditions.

SIMS focuses a primary ion beam to bombard the surface, causing the ejection of sputtered secondary ions. The secondary ions are by mass spectroscopy in which elements are accelerated through a magnetic field to determine their weight. The advantages of this technique

are the small sputtering depth, <100 nm, the range of elements capable of being detected (which is the largest of all techniques), and the sensitivity capable of detecting most elements with elemental concentrations between 10^{16} cm^{-3} and 10^{18} cm^{-3}. However, the disadvantage is the destructiveness of the sputtering, which may prevent additional use of the sample.

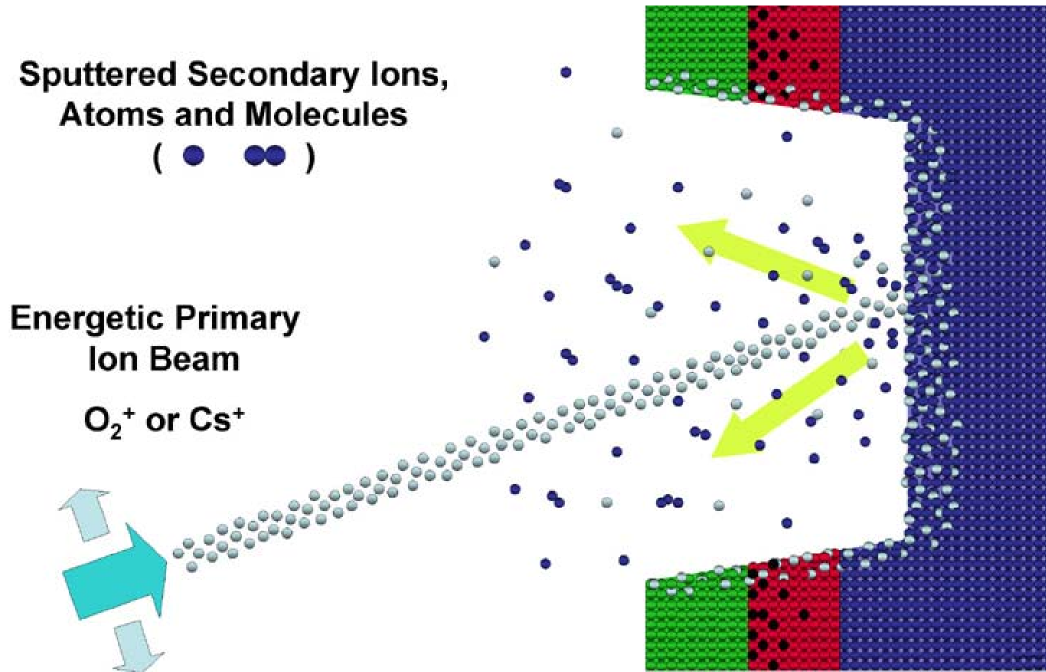

Figure 2.6: Depiction of primary ion sources bombarding the multiwalled surface of the sample; charging can also be seen as the primary ions spread through the films.

2.5.4 Micro Raman Spectroscopy

Raman spectroscopy was performed by the Naval Research Laboratory. Raman spectroscopy is a very useful tool, due to its ability to distinguish between SiC polytypes and determine elemental concentrations within a crystalline structure. In this paper it was used to distinguish between polytypes formed during epitaxial growth with increased C/Si ratios.

Raman spectroscopy characterizes molecular vibrations by inelastic light scattering known as the Raman Effect. This is done by focusing a laser, ~1 µm in diameter, at the surface of the sample, which interacts with phonons at the surface altering the state and energy of the laser photons. The change in energy is collected using an oscilloscope, which is capable of analyzing intensities of refracted wavelengths. The uniqueness of vibrational wavelengths allows for direct interpolations of various polytypes. However Raman spectroscopy is not capable of identifying element types, but a means of distinguishing between vibrational energies.

CHAPTER 3 - Results and Discussion

3.1 In-situ Hydrogen Etching

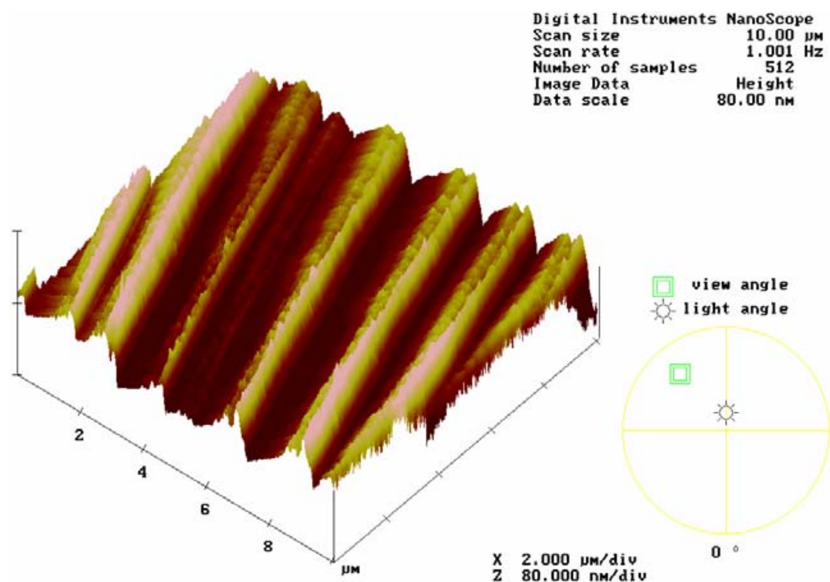

Figure 3.1: Step bunching caused on on-axis 4H-SiC after in-situ hydrogen etching. The sample shown was etched for 15 minutes at 1700 ˚C; step heights are approximately 75 nm.

Hydrogen etching of the SiC substrate is a very common procedure performed in the reactor prior to epitaxial growth. It smooths the surface by removing polishing scratches to produce regular features which help promote defect-free epitaxial growth. Surface etching of SiC begins near 1500 °C on 8° off-axis 4H-SiC, with the intent of producing the smoothest surface with regular step features.[39] Etching conditions on on-axis SiC may be different, since there are no step features on the surface and "step bunching" features may form. The presence of step bunching on on-axis SiC occurs after etching above 1500 °C, as shown in Figure 3.1.[40,41] Therefore reports of on-axis hydrogen etching are mentioned to be optimal at lower temperatures to produce the smoothest surface[42]. Though it produces smooth surface on off-axis SiC, there have been no reports of how post-hydrogen etching surface roughness affects subsequently grown on-axis SiC epitaxial layers.

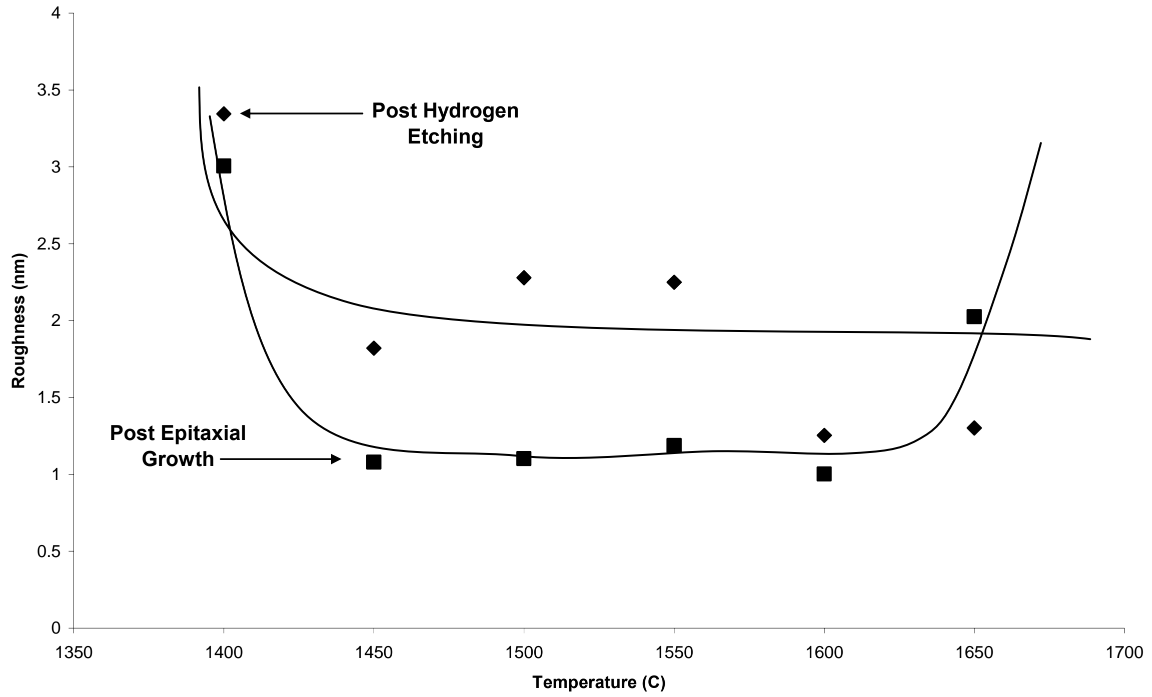

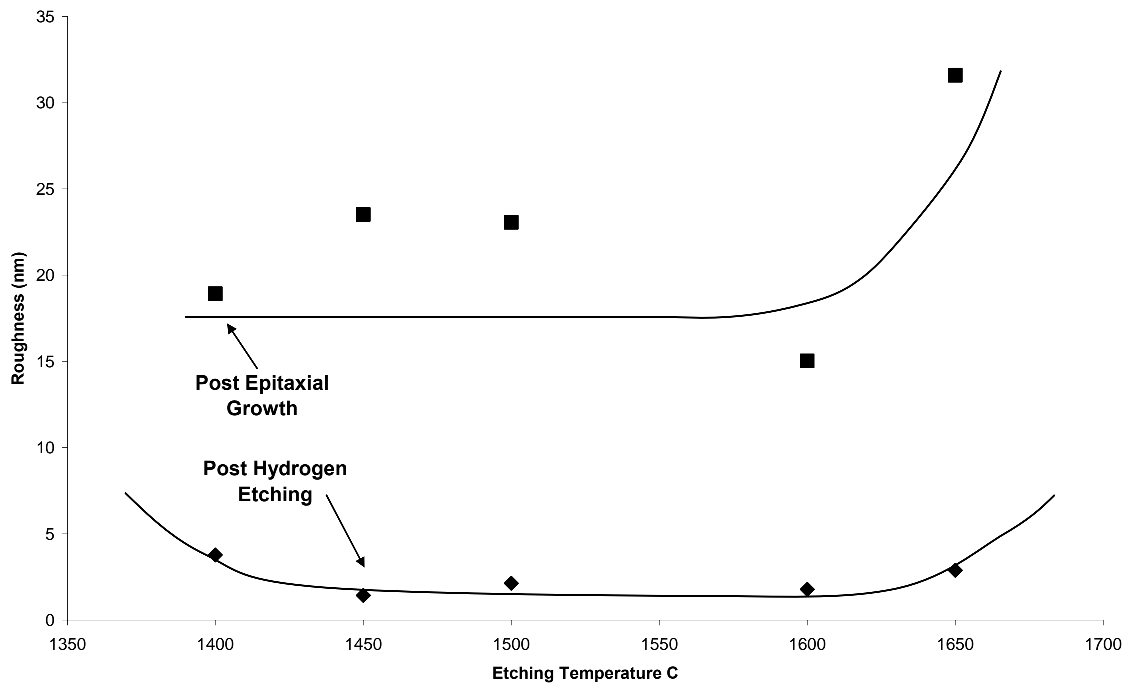

Figure 3.2: 4H-SiC on-axis average surface roughness, for 10 µm x 10 µm area after in-situ hydrogen etching and epitaxial growth.

The impact of hydrogen etching of on-axis substrates on the roughness of subsequently grown 4H-SiC homoepitaxial layers was investigated. The purpose of these experiments was to determine the optimal temperature for hydrogen etching of on-axis SiC substrates. To do so, SiC substrates were etched using 2 slm of hydrogen at 800 torr for ten minutes. Etching was conducted from 1400 °C to 1650 °C, after which the roughness of each substrate was measured using AFM. An epitaxial layer was then grown on each substrate for 20 minutes, using a 0.4% MTS fraction in a total flow of 2 slm hydrogen. The growth temperature was 1650 °C for all samples, with a system pressure of 200 torr. The surface roughness of each epitaxial film was then measured for comparison.

Two plots, summarizing the surface roughness after etching and sequential epitaxial growth are displayed in Figure 3.2, as measured by AFM on on-axis 4H-SiC substrates. For both the epitaxial films and hydrogen etched substrates, the roughness was lowest for samples etched between 1450 °C and 1600 °C. Therefore optimal etching conditions for both the carbon and silicon polarities occur near 1550 °C, as this produce the smoothest epitaxial surface. The surface roughness of the samples increased to ~2 nm on both polarities, after etching compared to the roughness of the polished wafer, ~0.6 nm, due to the formation of “step bunching”. Furthermore, the roughness of the epitaxial films grown on silicon polarities decreased by an average of 0.6 nm, where on carbon polarities it increases by an average of 15 nm compared to the post hydrogen etching roughness. On a lower magnification encompassing a larger area, Figure 3.3, the epitaxial surface is not smooth and therefore the roughnesses reported are representations of localized growth.

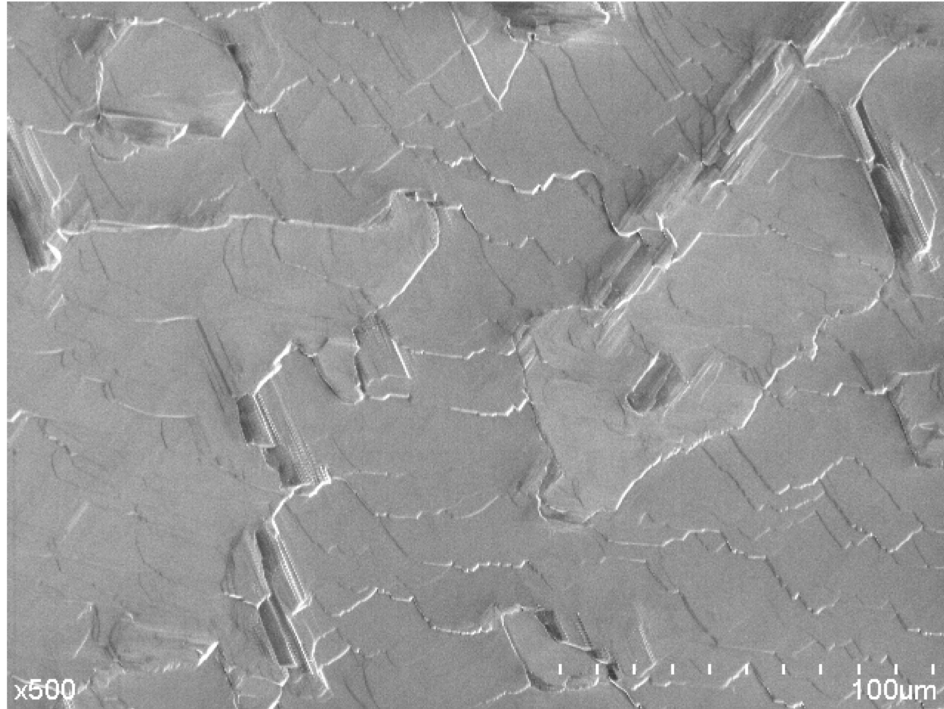

Figure 3.3: SEM image of step-like surface features seen on on-axis 4H-SiC epitaxial growth, grown at 1650 ˚C with an approximate film thickness of 13 µm.

The increased surface roughness of the substrates after hydrogen etching at higher temperatures is due to the formation of step bunching. This is caused by over etching of the material, which may result in an increased epitaxial film surface roughness. In general, polishing scratches on the carbon polarity are deeper than those on silicon polarity. It is also more reactive and etches faster, which removes the deeper polishing scratches but may also over etch the surface faster. This can be deduced from the greater roughness of the substrate surface and larger step features at high and low temperatures, as compared to the silicon face. The increased roughness of the epitaxial film of the carbon polarity is due to the decreased surface mobility of reactants; they are prevented from finding areas of lowest potential, causing polycrystalline SiC growth.

3.2 Temperature

Temperature is one of the most dominating attributes associated with CVD epitaxial growth. It has the ability to affect both the growth rate and surface morphology of the epitaxial films. Therefore, understanding of how this parameter affects such attributes is important. To study this, epitaxial growth experiments were run over a range of temperatures from 1600 °C to 1800 °C. The remaining growth conditions were fixed for all one hour runs, using 1 slm H_2, 2 sccm MTS and 200 torr. Each experimental run was done using two 5 mm x 10 mm 4H-SiC on-axis substrates, with growth on either the silicon or carbon polarities.

3.2.1 Growth Rate

The growth rate was determined by two different methods, by weight change and cross-sectional measurement. The layer thickness was calculated by weighing the sample before and after epitaxy, using a Texas Instruments analytical balance capable of measuring 0.0001 g. The difference in weight can then be divided by the density of the material and surface area of the substrate. The resulting solution represents the thickness of the epitaxial film, when uniform epitaxy is achieved.

$$\Delta weight \cdot \frac{1}{density \cdot S.Area} = Thickness \qquad (3.1)$$

To directly measure the thickness of the epitaxial films, each substrate was cleaved (near the center) using a diamond scribe. Samples were loaded into the SEM such that the cross-section were facing the detector. The thickness of the epitaxial film was evident from the difference in color, caused by variation in dopant concentration. Analysis equipment was then used to accurately measure the thickness of the epitaxial film. Figure 3.4 shows the cross-sectional cleavage and thickness. This measurement can be compared to the weight calculation, using equation 3.1, of the same sample shown below. The ability to determine the epitaxial film thickness by both calculation and direct measurement, allows for a comparison of film uniformity. For example, comparing the thickness calculated above from equation 3.1, 14.9 μm, to that of the SEM measured value in Figure 3.4, 14.83 μm, shows that this particular epitaxial film has a relatively uniform thickness across the surface.

$$[0.1495g - 0.1543g]\frac{1}{3.22\frac{g}{cm^3}\cdot 1cm^2} = 0.001491cm = 14.9\mu m \pm 0.6\mu m$$

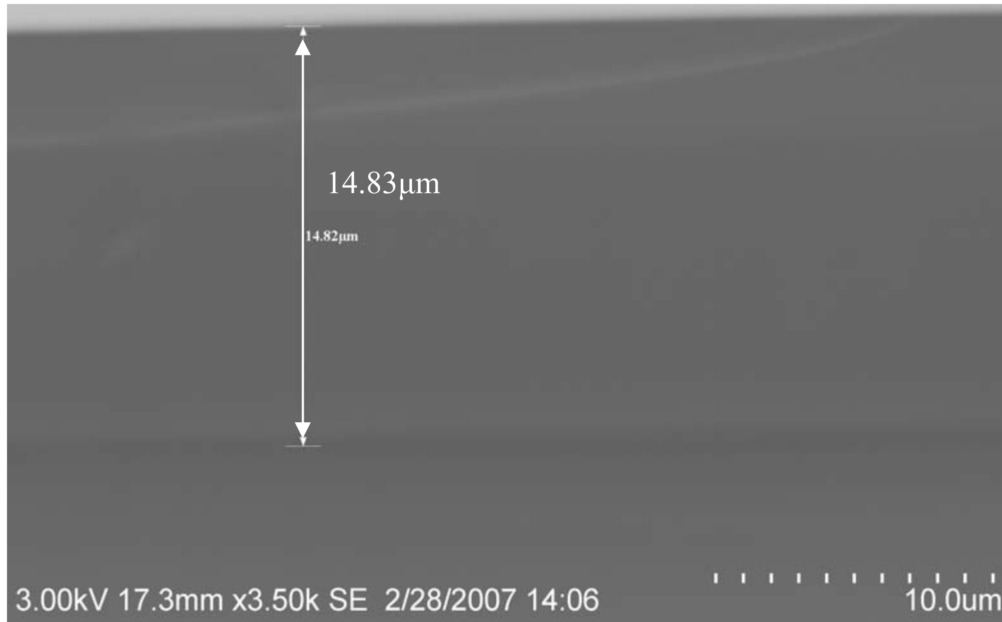

Figure 3.4: Cross-sectional SEM of C-face epitaxial film on on-axis 4H-SiC, ~14.83 µm±.05 µm.

Figure 3.5 displays the epitaxial growth rates over a range of temperatures from 1600 °C to 1800 °C. The reactant flow rates were fixed for all experiments at 3.8 slm hydrogen and 1.8 sccm MTS. The temperature has a large effect on the uniformity of the film thickness. For example, at low temperatures, ≤ 1700 ºC, the film thickness appears to be relatively uniform, with an average difference in thickness of 1.7 µm, on both the carbon and silicon polarity substrates. As seen in this figure, that the maximum uniform growth rate on both carbon and silicon polarities occurs between 1650 ºC and 1700 ºC (0.520 and 0.506), at a rate of ~12 µm/hr.

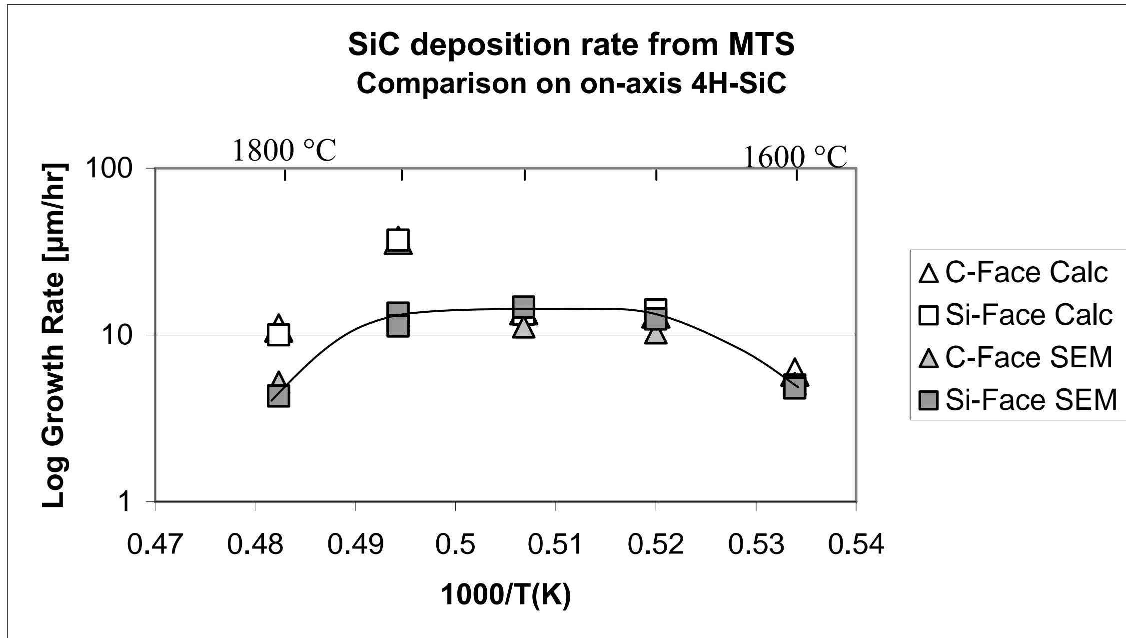

Figure 3.5: Effect of temperature on deposition rate using on-axis 4H-SiC with an MTS molar fraction of 0.05%.

The inability to deposit uniformly thick films and to increased growth rate at higher temperatures could be due to warping of the substrate or gas phase nucleation. Warping of the substrate is always a concern for epitaxial growth in cold wall reactors and is the most likely cause of nonuniform film thicknesses. The increased temperature at the center of the substrate causes reactant species to migrate to the cold regions, edges and corners, for deposition. Precautions were taken to help prevent this, such as using smaller substrates and slow heating of the substrate to reaction temperature. Gas phase nucleation would not be responsible for the nonuniform film growth, but can explain the decrease in growth rate at high, ≥1750 °C, and low, ≤1600 °C, temperatures. Gas phase nucleation can occur from the decomposition of volatile silicon compounds into silicon and the formation of silicon carbide in the gas phase, reducing the amount of reactants available for epitaxial growth. The presence of chlorine in the reaction phase can help reduce the formation of silicon; however it may not prevent the formation of SiC in the gas phase. Another possible explanation of the decreased growth rates above 1750 ºC and below 1650 ºC, is that at lower temperatures the system may be limited by reaction rate and at higher temperatures by SiC decomposition and etching from HCl, as observed in gallium arsenide epitaxial growth.[49]

3.2.2 Surface Morphology

The surface morphology of the epitaxial layer was highly dependent on the reaction temperature. Figure 3.6 shows three SEM images of the surfaces of the epitaxial layers reported in the previous section. At 1600 ºC silicon droplets are present across the surface of the epitaxial film. Between 1650 ºC and 1750 ºC, silicon was absent on the epitaxial surface. At 1650 ºC the surface appears to be covered with polycrystalline SiC, which will be further discussed in the following section. At 1750 ºC and higher, large, individual SiC crystals were randomly oriented on the surface.

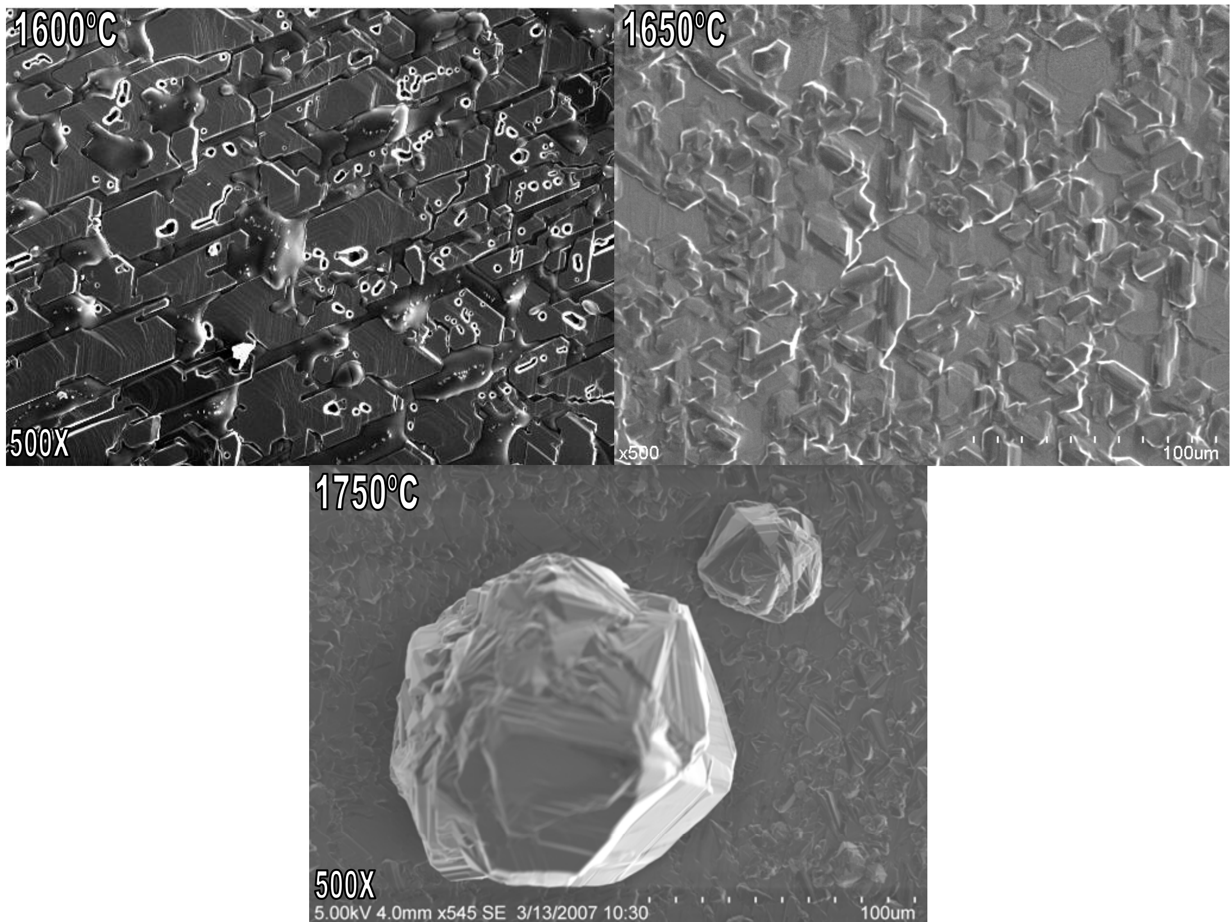

Figure 3.6: SEM images, magnified 500x, of on-axis 4H-SiC (Si polarity) epitaxial layers grown with 1 slm H_2, 4 sccm MTS.

The presence of silicon droplets and large SiC crystals proves that gas phase nucleation did occur during epitaxial growth; the use of a chlorinated precursor did not prevent their formation. The formation of silicon at lower temperatures is due to the undesired decomposition of volatile silicon compounds in the gas phase, similar to growth with silane and propane. On

the other hand the gas phase nucleation of SiC is most likely due to recirculation in the reactor, caused by large temperature differences. The large SiC crystals appear to be polycrystalline without any preferred orientation, suggesting they nucleated in the gas phase. Therefore, to prevent gas phase nucleation the growth temperature should be kept between 1650 ºC and 1700 ºC.

3.3 MTS Molar Fraction

The mole fraction of MTS in the carrier gas controls the growth rate and surface morphology of the epitaxial films. To understand the affect of MTS mole fraction on epitaxial growth on on-axis substrates, experiments were run varying the MTS fractions (in the carrier gas) from 0.02% to 0.10%. The carrier gases had a total flow rate of 4.5 slm over a range of hydrogen-to-argon ratios of 0.1 to 0.3. The different hydrogen to argon ratios tested the effect of hydrogen concentration on the decomposition of MTS and thus the growth rate. Additional epitaxial films were grown on 4H-SiC 8º off-axis substrates with a H_2/Ar ratio of 0.1 over the same range of MTS fractions. All experiments were run at 1650 ºC at a system pressure of 200 torr and reaction time of 60 minutes. Epitaxial growth was done on the silicon polarity of 4H-SiC (0001) substrates. Since epitaxial films grown at 1650 ºC are uniform in thickness, all thicknesses and growth rates reported for these experiments were determined by weight change calculations.

3.3.1 Growth Rate

Figure 3.7 shows the growth rate linearly depended on the mole fraction of MTS in the carrier gas and was independent of the hydrogen-to-argon ratio. The decomposition of the MTS can occur without high concentrations of hydrogen in the carrier gas. Low concentrations of hydrogen are beneficial in preventing decomposition of the graphite heating element. Since the concentration of hydrogen doesn't affect the decomposition of MTS, the growth rates achieved are the maximum possible growth rates on on-axis 4H-SiC.

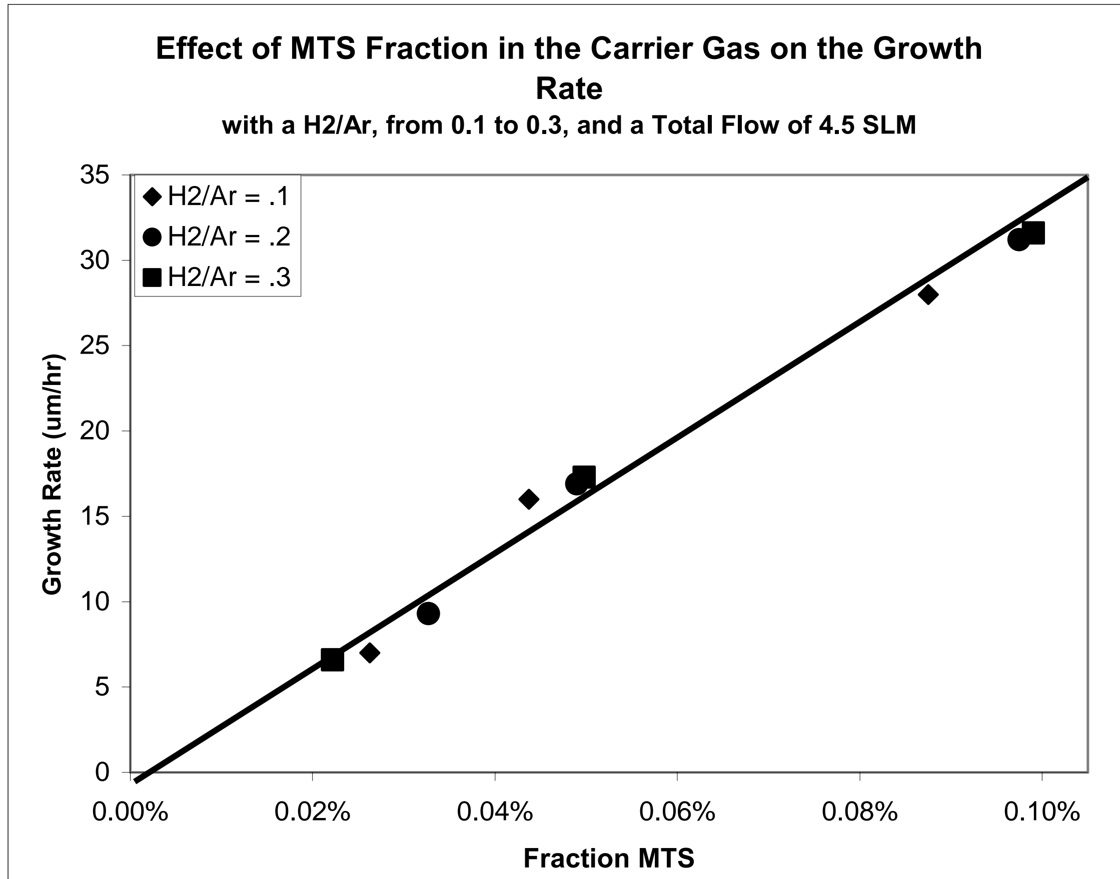

Figure 3.7: Effect of MTS mole fraction and total flow rate on the deposition rate using on-axis 4H-SiC substrate at a growth temperature of 1650ºC.

The epitaxial growth on on-axis and 8º off-axis 4H-SiC substrates were compared to show how the presence of "step growth" epitaxy affects the growth rate. The relationship of growth rate and MTS mole fraction are similar for both orientations, therefore "step growth" does not affect the overall growth rate. These results were compared to similar experiments performed by Pedersen *et al*[35]; the growth rates determined in this study were slightly lower; but followed the same linear trend. Thus it can be inferred that the linear relationship is correct.

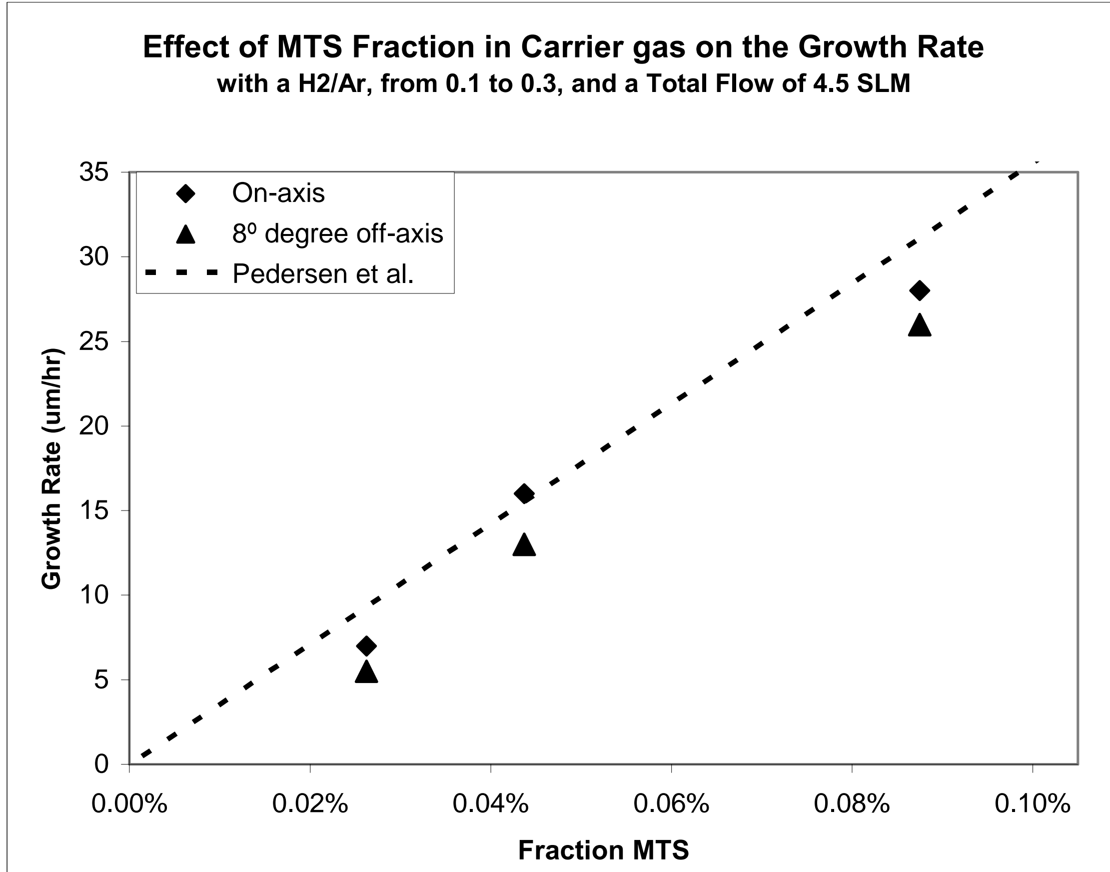

Figure 3.8: Comparison of 4H-SiC on-axis and 8º off-axis epitaxial growth rates to that reported by Pedersen, *et al (2007)*.

3.3.2 Surface Morphology

The ability to produce smooth, uniform epitaxial films is required for electronic device manufacturing. Therefore, the surface morphology of the SiC samples used to generate Figure 3.8, were studied to determine the effect of "step growth" epitaxy versus terrace growth, and are presented in Figure 3.9. In this figure, the morphologies of epitaxial films on on-axis and 8º off-axis 4H-SiC substrates are compared. The samples are displayed from top to bottom with increasing MTS mole fractions, from 0.025% to 0.09%. Low MTS molar fractions, ~0.025%, produce a growth composed primarily of polycrystalline SiC on on-axis substrates and a relatively smooth epitaxial layer on off-axis substrates. Increasing the mole fraction to approximately 0.05% improved the quality of the epitaxial layer on the on-axis substrate by producing mixed polycrystalline growth and epitaxial growth. However on this sample the epitaxial layer is not smooth, but covered with "step bunching" features. At the highest mole

fraction, 0.09%, the surface quality of both the on-axis and off-axis morphologies decreased. The on-axis substrate converted back to a complete polycrystalline deposit, whereas the film on the off-axis substrate had large-comet shaped features.

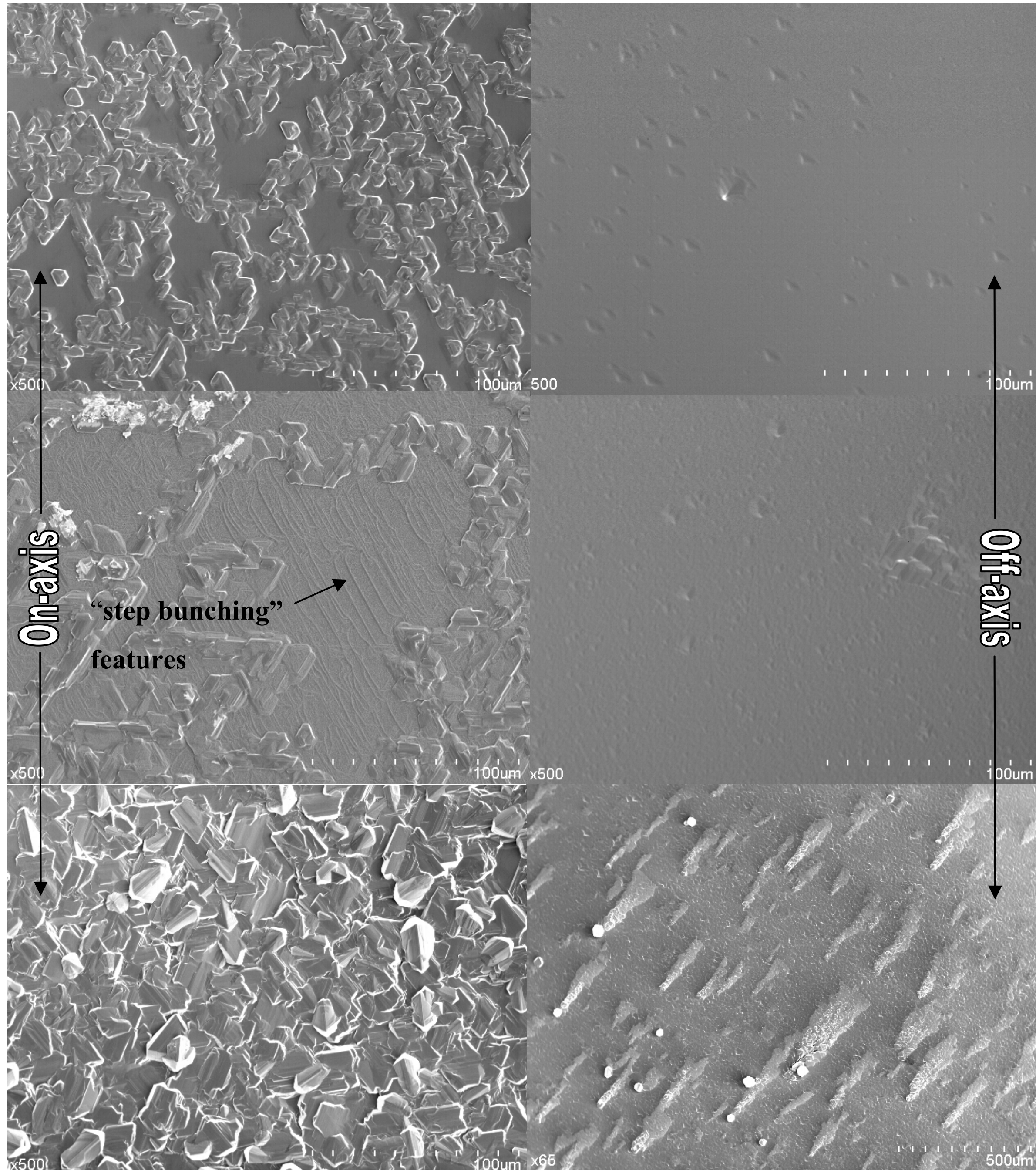

Figure 3.9: SEM images of 4H-SiC epitaxial films grown at 1650°C with a H_2/Ar of 0.1; Left: on-axis substrates, Right: 8° off-axis; MTS mole percents Top: ~0.025%, Middle: ~0.05%, Bottom: 0.09%, all images are displayed at 500X.

The formation of polycrystalline SiC demonstrates the difficulty associated with epitaxial growth on on-axis 4H-SiC substrates. At low mole fractions small amounts of polycrystalline growth occur without fully covering the surface. On the other hand, the polycrystalline growth at high molar fractions is probably caused by the presence of gas phase nucleation, which can also be seen on the off-axis substrate as the head of the comet shaped features. The tails of these features occur in perpendicular to the steps, in the (11-20) direction, suggesting growth also occurs in that direction. In summary, the use of 0.05% MTS molar fraction produces the best epitaxial film for on-axis 4H-SiC growth.

3.3.3 SIMS

Secondary ion mass spectroscopy was performed on two epitaxial films, one silicon polarity, the other carbon polarity, grown on on-axis 4H-SiC. The concentrations of residual boron, aluminum and nitrogen impurities were measure. Table 3-1 summarizes the results obtained from the SIMS analysis, performed by Evan's analytical group. Analysis depth for these results was approximately 2 nm. Nitrogen incorporation appears to be higher on the carbon polarity, whereas boron increases on the silicon polarity. This is consistent with the "site competition theory", such that n-type elements (nitrogen) replace carbon and p-type elements (boron) replace silicon in the lattice structure.

Table 3-1: Summary of test results obtained for the impurities of nitrogen, boron and aluminum [atoms/cm^3] in two epitaxial films grown at 1650 °C, 3.55 slm Ar, 350 sccm H_2, and 2.25 sccm MTS (0.05%).

Polarity	B	Al	N
Carbon	9.6×10^{14}	1.5×10^{14}	5.1×10^{18}
Silicon	1.2×10^{16}	1.5×10^{14}	1.5×10^{15}

3.4 Defects

The propagation of defects through the epitaxial layer degrades its electrical properties, which can prevent its use for electronic devices. Defects that propagate through the epitaxial film typically start from a micropipe (MP), which are large hexagonal holes, or basal plane dislocation (BPDs), in the substrate.[43,44] The larger the misorientation angle of the off-axis substrate, toward the a-axis, the greater the chance that defects will propagate through the epitaxial film to the surface.[47] In some cases however these defects can be converted into other types of defects during epitaxy, propagating through as threading edge (TED) or screw dislocations (SD), which are much less deleterious for device operation. Epitaxial growth on on-axis substrates is capable of converting nearly 100% of BPD and MP into TEDs and SDs.[28]

Not all defects originate from the substrate; some are created during epitaxy. These defects including change in polytype (as inclusions or stacking faults) and polycrystalline growth. Typically on-axis SiC growth defects are associated with 3C-SiC inclusions, which can be characterized by the triangular shape of the micropipe defects. However, these defects can also propagate from gas phase nucleation as silicon droplets or as raised comet shape features, as seen previously in Figure 3.9.

3.4.1 Defect Selective Etching

Defect selective etching in molten KOH, is used to locate and identify edge, screw and mixed dislocations, stacking faults and other defects. It can be applied to either surfaces or cross-sectional edges of crystals. For this study, all sample orientations were etched for two minutes using molten potassium hydroxide at 500 ºC. Figure 3.10 shows the cross-sectional view of an on-axis 4H-SiC epitaxial film, where a) displays horizontal and vertical stacking faults and b) stacking faults from “step bunching”. Stacking faults can be seen propagating vertically, horizontally and diagonally. Stacking faults are caused by mistakes in regular stacking sequence, such as a localized band of polytype. The presence of both vertical and horizontal stacking faults suggests that growth is taking place in both the vertical and horizontal directions. The diagonal stacking faults appear to form triangular shapes which increase in size with the thickness of the epitaxial film. The triangular defects first suggest the presence of 3C-SiC due to the 3-fold symmetry; however, these triangular shapes are caused by step bunching that occurred during in-situ hydrogen etching.

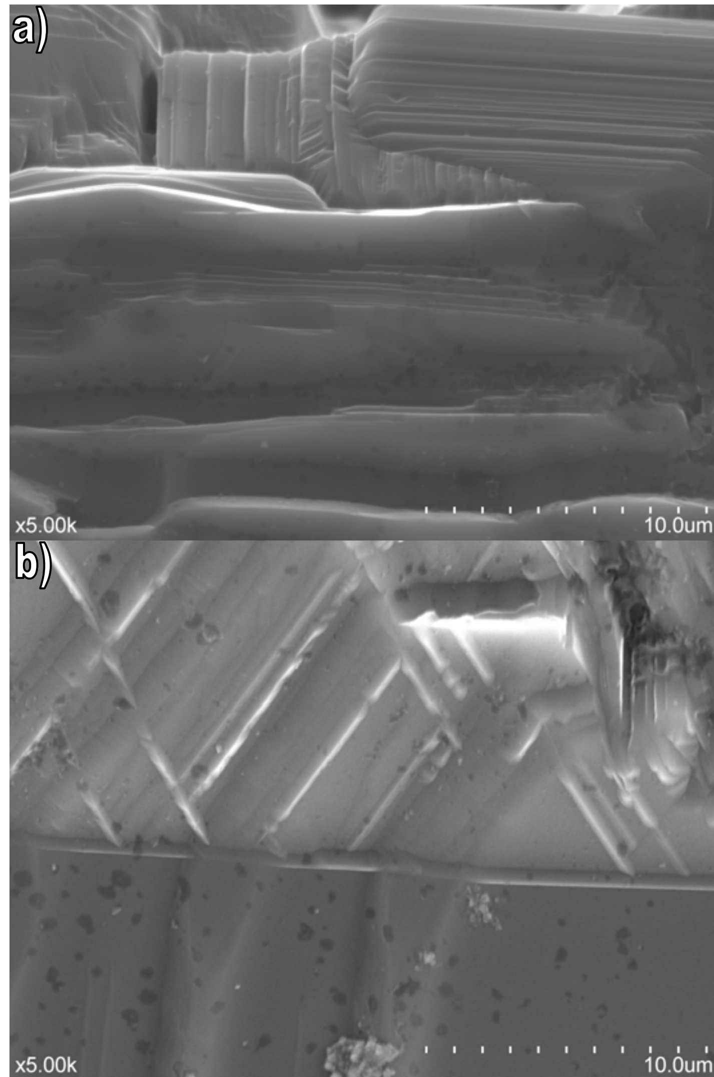

Figure 3.10: Stacking faults formed during 4H-SiC on-axis epitaxial growth; a) vertical and horizontal stacking faults, b) "step bunching" stacking faults.

Molten KOH etching also produces large hexagonal pits within 4H-SiC epitaxial films on on-axis substrates, as shown in Figure 3.11. It appears as though the epitaxial film, B, grew inside and around a MP defect in the substrate, A. However it also appears as though the epitaxial growth covered or completely filled the MP, C. This suggests that on-axis epitaxy converts or prevents the propagation of MP through the epitaxial film, such as the fill MPs labeled "C". Though on-axis substrates were used, there is always a slight misorientation toward the a-axis. The oval shaped tail around these etch pits are assumed to be perpendicular to the misorientation.

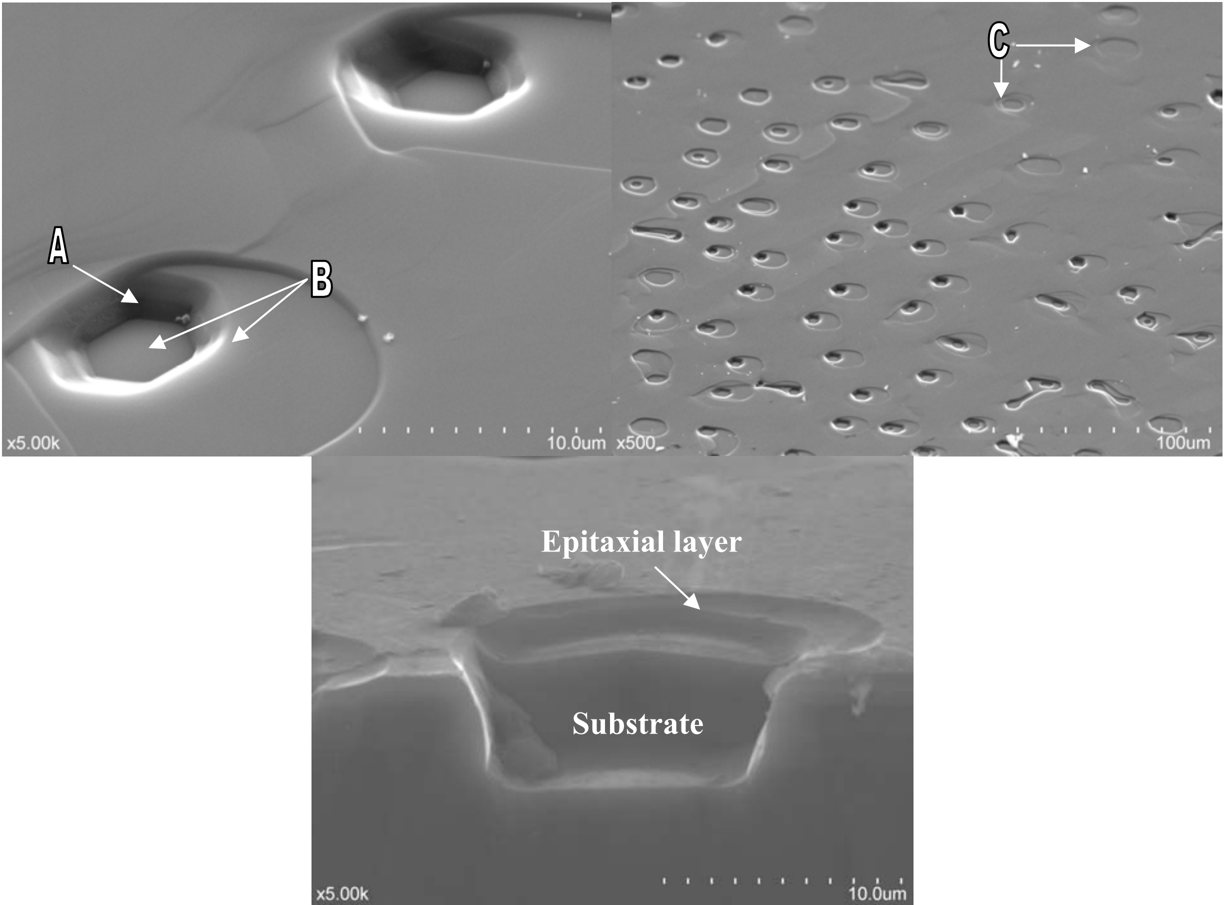

Figure 3.11: Etch pits reviled after etching in potassium hydroxide, showing epitaxial growth of the same epitaxial film at different magnifications and regions; A: substrate, B: Epitaxial growth and C: Completely fill MPs.

3.4.2 Silicon Droplets

Figure 3.12a, shows an SEM image of silicon droplets, covering ~60% of the surface, deposited on the surface of an on-axis 4H-SiC epitaxial film. The growth took place at 1650 ºC and 200 torr with a MTS flow rate of 1 sccm and carrier gas flow rate of 2 slm H_2. The presence of chlorine during epitaxial growth should have suppressed the gas phase nucleation of silicon. Therefore we hypothesized that the silicon droplets nucleated from a defect in the epitaxial film. To examine this hypothesis, selective etching was done to remove silicon without etching the SiC. Samples were submerged in 27% acetic acid, 27% hydrofluoric acid and 45% nitric acid at room temperature, for 20 minutes. The silicon droplets were successfully etched from the surface, leaving behind what appeared to be polycrystalline SiC (Figure 3.12b). These samples, cleared of silicon were subsequently etched in molten potassium hydroxide to selectively etch

the polycrystalline SiC and defects in the epitaxial film. The results are shown in Figure 3.12. Defect selective etching of this surface revealed very large areas, ~5 mm^2, which were defect free, with an average surface roughness of 2.3 nm and epitaxial thickness of 5 μm. The average etch pit density was approximately 10 cm^{-2}, compared to 60 cm^{-2} of the substrate. The etch pits on these samples were composed of hexagonal shaped etch pits, suggesting the epitaxial film is composed 4H-SiC.

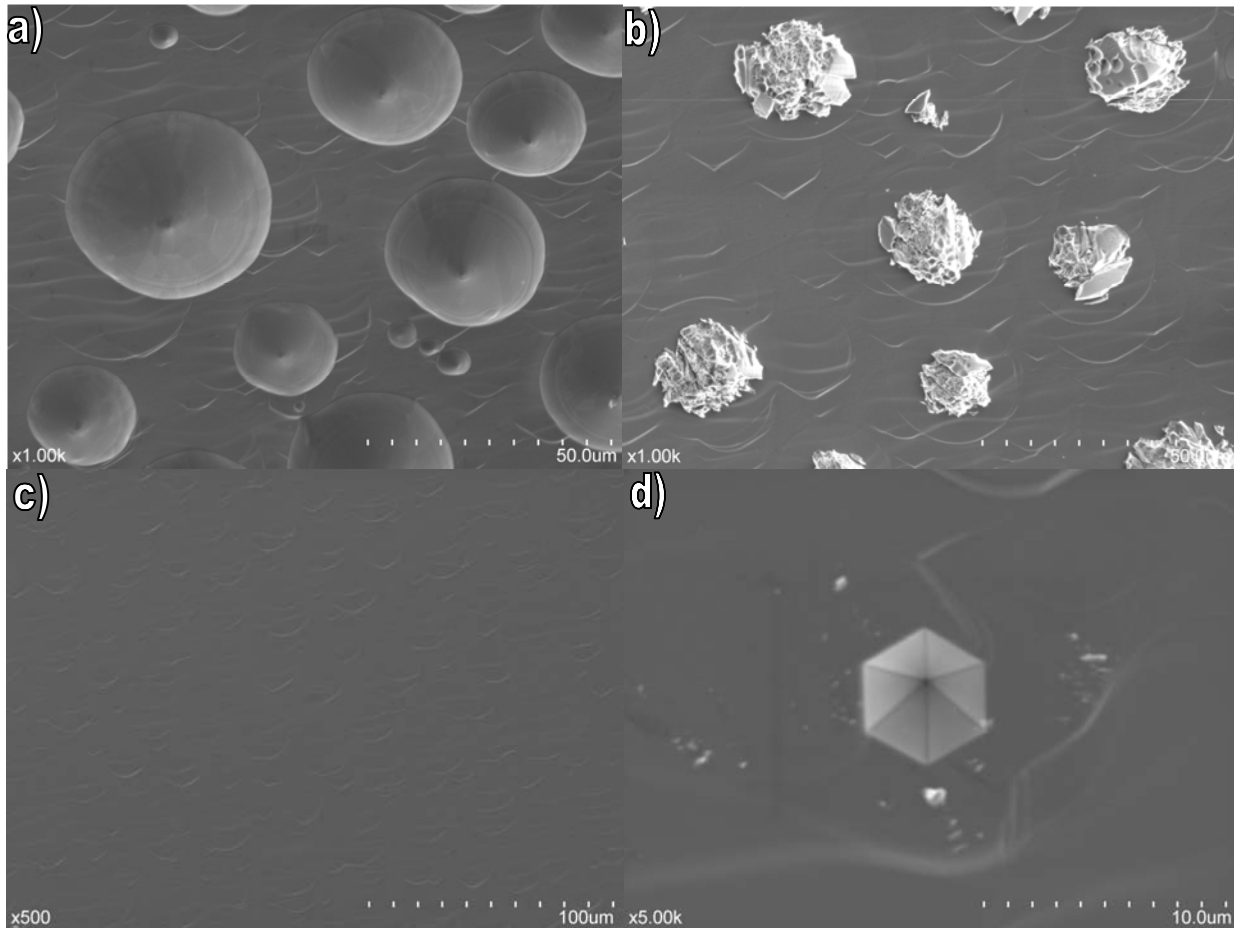

Figure 3.12: SEM images of on-axis epitaxial growth that resulted in the presence of silicon droplets and homogenous 4H-SiC epitaxy on on-axis 4H-SiC (all images from same sample); a) after epitaxial growth, b) after HNA etch, c) after KOH etch, d)Threading edge dislocation (5k magnification).

The absence of etch pits forming in the epitaxial film proves that the silicon droplets do not propagate from or nucleate from defects. Therefore the presence of silicon droplets on the surface are due to the undesired decomposition of volatile silicon compounds into silicon. Only experiments run with low molar fraction of MTS, ≤0.05%, in pure hydrogen produce silicon.

This is possibly due to the high concentration of hydrogen forcing MTS to decompose into silicon, methyl radicals or methane, and hydrogen chloride. The presence of polycrystalline SiC revealed after removal of the silicon may indicate that some carbon compounds dissolved into the silicon droplets and precipitate as SiC within the silicon. Since the presence of the silicon and polycrystalline SiC had no effect on the quality of the epitaxial film, the polycrystalline SiC formed during the gas phase nucleation process and deposited during cool down.

Not all epitaxial films containing silicon depositions had relatively smooth epitaxial films. Figure 3.13 shows SEM images of SiC epitaxial growth on on-axis 4H-SiC at a lower temperature, 1500 °C, than the previous samples discussed. The triangular shaped micropipe, propagating through the film, suggests the film was 3C-SiC. Film growth was determined to be approximately 3 μm by cross-sectional clevage. The low temperature and cubic crystalline structure proves that the film is composed of 3C-SiC.

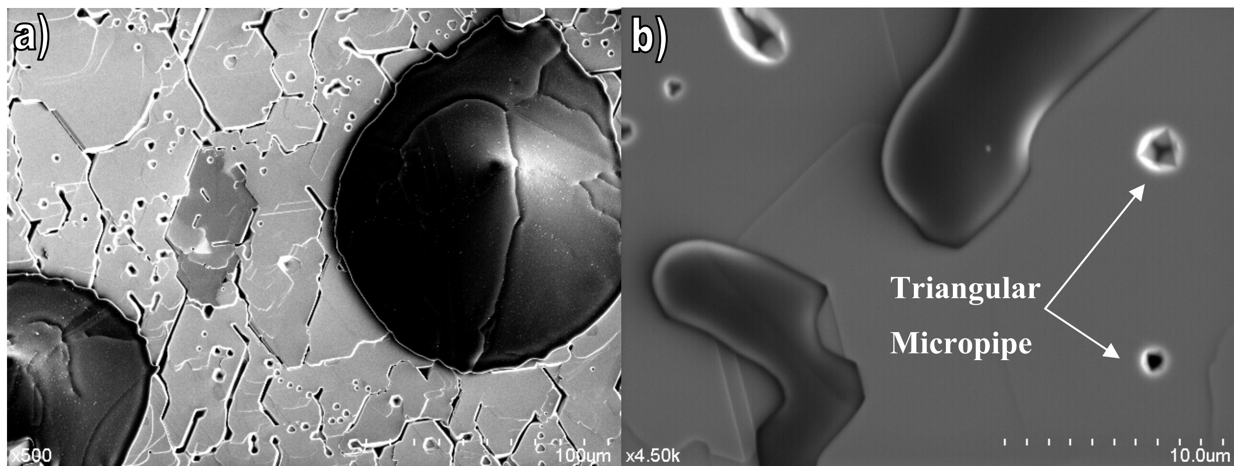

Figure 3.13: On-axis 4H-SiC epitaxial growth at 0.05% MTS, 2 slm H_2 and 1500 °C, causing the formation of 3C-SiC.

In an attempt to suppress the formation of silicon droplets, additional carbon was added using 1% ethane in argon to the reactant gasses. Experiments were run using the same conditions as above, but with an increased C/Si ratios of 2 and 3. The resulting samples produced with these conditions were covered with a black coating, most likely graphite, which was very soft and easily removed by scratching. Figure 3.14 shows an optical micrograph of the film grown using a C/Si = 3. The region in the bottom right-hand corner was scratched with a pair of tweezers, removing the graphite layer and reviling polycrystalline SiC, ~ 25 μm thick.

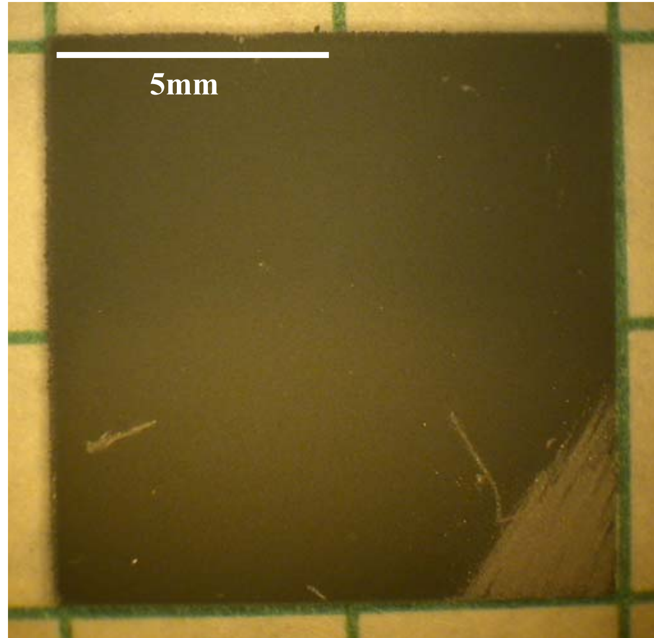

Figure 3.14: Optical micrograph of 4H- on-axis SiC with graphite deposition on silicon polarity, due to an increased C/Si ratio of 3, magnification was 20X.

Similar experiments using 4º off-axis 4H-SiC substrates produced similar results. These experiments suggest that an excess of carbon was present during deposition with additional ethane. To ensure the only additional carbon in the reactor was due to the ethane, argon was added to make a 1:1 ratio of $Ar:H_2$, and to help suppress the reaction of hydrogen with the heating element. The surface morphology of the SiC growths are shown in Figure 3.15. The higher C/Si ratio of 3 appears to have increased the quantity of features, but decreased the overall size and quality as a single crystalline structure. This suggests the growth rate was increased with respect to the increased C/Si ratio. Samples were sequentially etched using molten potassium hydroxide for five minutes to etch away the defects; however, the structures remained unchanged, proving these features are SiC.

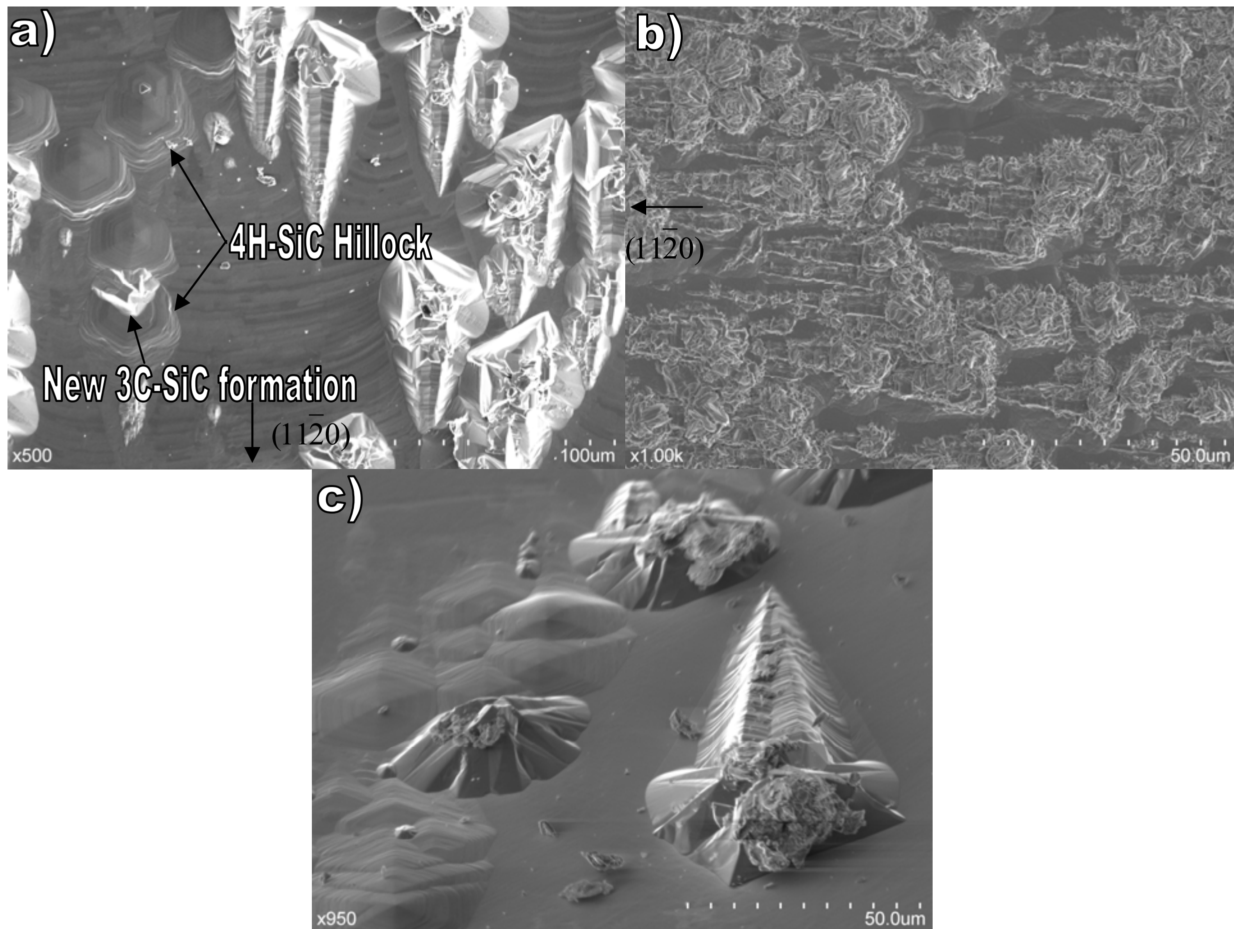

Figure 3.15: SEM images of 4H-SiC 4º off-axis SiC epitaxial layer and growth defects, with H_2:Ar of 1:1; a) and c) C/Si = 2, b) C/Si = 3.

The observed cone-shaped features formed during SiC epitaxial growth have not been previously reported in literature. However, these defects are similar to the "4H-SiC carrot defects" observed by *X. Zhang et al.*[48]; both are cone-shaped features with an over-size head, a triangular tail, and are oriented toward the $(11\bar{2}0)$ direction. The head of the defect is propagated from a threading dislocation, the body from a prismatic fault and the tail from a stair-rod dislocation. Raman analysis, shown in Figure 3.16b and c, of a single cone-shaped defect and surrounding region, shows that the defects are 3C-SiC. The surrounding hillocks (raised regions) are 4H-SiC. A photoluminescence micrograph shows that the hillocks propagated from threading dislocations (Figure 3.16a). Therefore it can be hypothesized, that the head of the cone starts as 4H-SiC hillock growth, Figure 3.15a, and then sequentially 3C-SiC growth on top. Thus, agreeing with the proposed propagation method of "carrot defects" described by *X. Zhang et al.*[48]

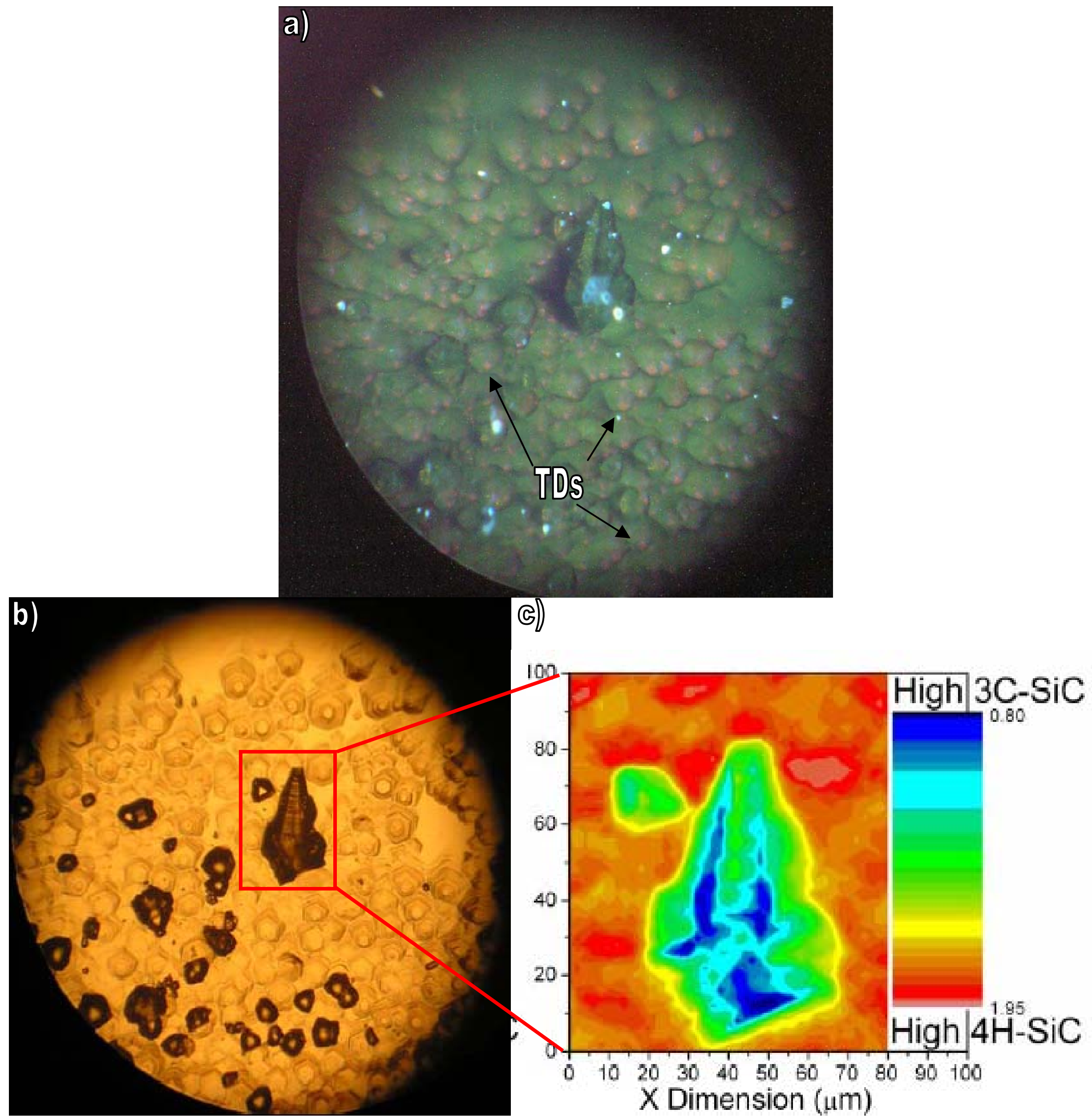

Figure 3.16: a) Photoluminescence micrograph of cone-shaped defect and surrounding area showing TDs in red; b) Reflected white light optimal micrograph of cone-shaped defect; c) Micro Raman spectral analysis of defect and surrounding region, distinguishing between 3C-SiC and 4H-SiC polytypes.

CHAPTER 4 - Conclusion

The purpose of this research was to determine a procedure for homoepitaxial growth of 4H-SiC on on-axis 4H-SiC using a chlorinated precursor. On-axis wafers are lower cost than off-axis wafers, as less of the high quality boule is wasted. On-axis wafers are also capable of converting micropipes and basal plane dislocations into threading edge and screw dislocations in the epitaxial films. However, epitaxial growth is far more difficult on on-axis wafers due to the growth of 3C-SiC inclusions and polycrystalline SiC.

In this study methyltrichlorosilane was chosen as a single precursor for epitaxial growth of silicon carbide, except when an increased C/Si ratio was used, in which 1% ethane in argon was added. A chlorinated precursor was used to reduce the presence of 3C-SiC inclusions by etching deposits during epitaxial growth. It is also believed to reduce gas phase nucleation of silicon and SiC, which can improve film quality.

Homoepitaxial films of 4H-SiC, as determined by hexagonal etch pits, on on-axis 4H-SiC were produced at low MTS mole fractions, 0.05%. The homoepitaxial film produced had reduced defect densities, 10 cm^{-3}, compared to that of the substrate, 60 cm^{-3}. However, silicon and SiC cluster deposits covered approximately 60% of the epitaxial surface, caused by gas phase nucleation. Additional selective etching steps were required to remove the silicon and poly-SiC deposits and uncover the entire surface. An increased C/Si was used to suppress silicon droplet formation, but was unsuccessful due to thick graphite coatings and polycrystalline deposition. Optimal etching temperature for on-axis 4H-SiC occurred from 1400 °C to 1600 °C, as determined by epitaxial surface roughness. Surface roughness after hydrogen etching proved that the carbon polarity is much more reactive, such that it etched much faster producing large "step bunching features". However growth rate was determined to be independent of surface polarity, with highest growth rate at 1650 °C.

The use of a chlorinated precursor on on-axis 4H-SiC, can produce homoepitaxial films by reducing the presence of 3C-SiC inclusions. However, the inability to prevent the formation of silicon by gas phase nucleation suggests the need for increased Cl/Si ratios. Therefore, future research should study the affect of increased Cl/Si ratios on-axis epitaxial growth. Additionally, homoepitaxial growth should be preformed on defect free wafers, when commercially available, to determine the effects of defects on epitaxial growth.

Appendix A - References

A.1 Cited Sources

1. Y. Shi, Z.Y. Xie, L. Liu, B. Liu, J.H. Edgar and M. Kuball, J. Crystal Growth **233** (2001), pp. 177.
2. G.L. Harris, in: G.L. Harris (Ed.), Properties of Silicon Carbide Inspec/IEE, 1995.
3. N. Ohtani; Springer, Berlin (2004), pp. 156
4. J. Takahashi; J. Crystal Growth **181** (1997) pp.229.
5. N.W. Jepps, T.F. Page, in: P. Krishna (Ed.), Progress in Crystal Growth and Characterization, **7**, (1983), pp. 259.
6. Kurt Nassau; Current Science, **79** (2000), pp. 11.
7. Juan Carlos Bulda, et al.; University of Arkansas <http://mixedsignal.eleg.uark.edu/sic/>.
8. E.R. Brown; Solid-State Electronics, **42** (1998), pp. 2119
9. J.B. Casady, R.W. Johnson, Solid-State Electronics. **39** (1996), pp. 1409.
10. Chow, T.P, Ghezzo.; Material Research Society Symposium Proceedings, Pittsburgh, PA. **423** (1996), pp. 69-73.
11. Goldberg Yu., Levinshtein M.E., Rumyantsev S.L. John Wiley & Sons, Inc., New York (2001) pp. 93-148.
12. Y.M. Tairov, V.F. Tsvetkov, J. Crystal Growth **43** (1978) pp. 209
13. M. Adams;< http://www.accuratus.com/silicar.html>.
14. W.F. Beadle, R.D. Plummer, and J.C.C. Tsui, *Quick Ref. Manual for Silicon Integrated Circuit Technology*, Wiley, New York, (1985), pp. 1-9
15. Khan, I.A, J.A. Cooper, Am. Sci. Forum **264-268** (1998), pp. 509-512
16. G.L. Harris, in: G.L. Harris (Ed.), Properties of Silicon Carbide Inspec/IEE, 1995
17. Kern, E.L., D.W. Hamil, H.W. Deam, H.D. Sheets, Mater. Res. Bull., Special Issue **4** (1969), S25-S32. Proceedings of the International Conference on Silicon Carbide, University Park, Pennsylvania, USA, October 20-23 1968.
18. G.L. Harris, in: G.L. Harris (Ed.), Properties of Silicon Carbide Inspec/IEE, 1995
19. Shaffer, P.T.B., J. Am. Ceram. Soc. **48** (1965), 11, pp. 601.

20. R.R. Reeber, K. Wang, Mater. Res. Soc. Symp. **622** (2000) T6.35.1.
21. Kh.S. Bagdasarov, E.R. Dobrovinskaya, V.V. Pishchik, M.M. Chernik, Yu. Yu, A.S. Gershun, I.F. Zvyaginstseva, Sov. Phys. Crystallgr. **18** (1973), pp. 242
22. NASA website; <http://www.grc.nasa.gov/WWW/SiC/benefits.html>.
23. J.A. Lely and Ber.Dt. Keram, Ges. **32** (1955), pp. 229.
24. Ritter, Steve; Chemical & Engineering News **82** (2004), pp. 35
25. Linkőpings Universitet, Material Science homepage; <http://www.ifm.liu.se/matephys/new_page/research/sic/ >.
26. Purdue University; <http://www.ecn.purdue.edu/WBG/Introduction/exmatec.html >.
27. Ritter, Steve; Chemical & Engineering News **82** (2004), pp. 35
28. Rong Jun Liu, ChangRui Zhang, XinGui Zhou and YingBin Cao; J. Crystal Growth **270** (2004), 1-2, pp. 124 – 127.
29. Yingbin ans Mark S. Gordon; J. Phys. Chem. A **111** (2007) pp. 1462 – 1474.
30. T. Ohno, H. Yamaguchi, S. Kuroda, K. Kojima, T. Suzuki, K. Arai; J. Crystal Growth **260** (2004) pp 209 – 216.
31. K. Kojima, H. Okumura, S. Kuroda, K. Arai, A. Ohi, and H. Akinaga; Material Science Forum, **483-485** (2005), pp. 93 – 96.
32. S.N. Gorin and L.M. Ivanova, Phys. Stat. Sol. (b) 202 (1997) pp. 221.
33. Peng Lu, Dissertation Kansas State University, unpublished (2006).
34. V.V. Zelenin, V.G. Solov'ev, S.M. Starobinets, S.G. Konnikov and V.E. Chelnokov, Semiconductors **29** (1995) pp. 581.
35. Larry B. Rowland, Canhua Li, Greg T. Dunne, Jody A. Fronheiser ; Mater. Res. Soc. Symp. Proc. **911** (2006), 0911-B09-01.
36. Hidekazu Tsuchida, Toshiyuki Miyanagi, Isaho Kamata, Tomonori Nakamura, Kunikaza Izumi, Koji Nakayama, R. Ishii, Katsunori Asano, Yoshitaka Sugawara.; Mater. Sci. Forum **483 – 485** (2005), pp. 97.
37. Pedersen, H., S. Leone, A. Henery, V. Darakchieva, E. Janzen; Surface & Coatings Technology **201** (2007), pp. 8931-8934
38. D. J. Larkin, Phys. Status Solidi B **202** (1997), pp 305

39. R. Yakimova, A.-L Hylen, M. Tuominen, M. Syvajarvi, E. Janzen; Diamond and Related Materials **6** (1997), pp. 1456 – 1458.
40. Subba Ramaiah Kodigala, I Bhat, T.P Chow, J.K. Kim, E.F. Schubert; Materials Science and Engineering B **129** (2006), pp. 22 – 30.
41. Christer Hallin, Igor Khlebnikov, Peter Muzykov, Elif Berkman, Monica Sharma, Geore Stratiy, Murat Silan, Cern Basceri, Cengiz Balkas; Mater. Res. Soc. Symp. Proc. **911** (2006), 0911-B09-05.
42. J.M. Harris, H.C. Gatos and A.F. Witt; Journal of Electrochem. Soc.: Solid State Science **116** (1969), pp. 672 - 673
43. K. Kojima, H. Okumura, S. Kuroda, K. Arai, A. Ohi, and H. Akinaga; Material Science Forum, **483-485** (2005), pp. 93 – 96.
44. Soubatch, S. , et al.; "Surface and Morphology of 4H-SiC Wafer Surfaces after H2-etching"; Material Science Forum; ECSCRM 2004.
45. S. Ha, P. Mieszkowski, M. Skowronski and L.B. Rowland; J. Crystal Growth **244** (2002), pp. 257 – 266.
46. T. Ohno, H. Yamaguchi, S. Kuroda, K. Kojima, T. Suzuki, K. Arai; Journal of Crystal Growth **271** (2004), pp. 1 – 7.
47. H.J. Rost, M. Schmidbauer, D. Siche, R. Fornari; J. Crystal Growth **290**, 1, pp. 137 – 143.
48. X. Zhang, S. Ha, M. Benamara, M. Skowronski, J.J. Sumakeris, S. Ryu, M.J. Paisely and M.J. O'Loughlin; Applied Physics Letters **85** (2004) 22, pp. 5209 – 5211.
49. D.H. Reep and S.K. Ghandhi, J. Electrochemical Society **130** (1983), pp. 675

A.2 Additional Sources

1. Francesco La Via, Giuseppa, Andrea Firrincieli, Salvatore Di Franco, Andrea Severino, Stefano Leone, Maarco Mauceri, Giuseppe Pistone, Giuseppe Abbondanza, Ferdinando Portuese, Lucia Calcagno, Gaetano Foti; Mater. Res. Soc. Symp. Proc. **911** (2006), 0911-B02-01.
2. Qiu Zu-min, Xiw Xin-liang, Lou Mei, Xie Feng-xia; Journal of Zhejiang University Science **6B** (2005), 6, pp. 559-562.
3. S. Amelinckx and G. Strumane; Journal of Applied Physics **31** (1960), pp. 8.
4. S. Kodambaka, S. V. Khare, W. Święch, K. Ohmori, I. Petrov and J. E. Greene; Letters to Nature **429** (2004). pp. 49 – 52.
5. T. Ohno, H. Yamaguchi, S. Kuroda, K. Kojima, T. Suzuki, K. Arai; J. Crystal Growth **260** (2004)., pp 209 – 216.
6. O. Kordina, J. P. Begman, A. Henery, E. Janzen; Appl. Phys. Letter **67** (1995) 11. pp 1561 – 1563.
7. P.H. Holloway; American Society for Testing and Materials (1980).
8. Paul K. Chu, Richard S. Hockett; Semiconductor International (1994), pp. 142 – 146.
9. Magnus Willander, Milan Friesel, Qamar-Ul Wahab; J. of Material Science: Materials in Electronics **17** (2006), pp 1 – 25.
10. Nick G. Wright, Alton B. Horsfall and Konstantin Vassilevski; Materials Today **11** (2008), 1 – 2.
11. M. Syväjärvi, R. Yakimova, E. Janzén; J. Crystal Growth **208** (2000), 409 – 415.
12. M. Syväjärvi, R. Yakimova, E. Janzén; J. Electrochem. Soc. **147** (2000), 9, pp. 3519 – 3522.
13. M. Syväjärvi, R. Yakimova, A-L Hylen, E. Janzen; J. Phys.: Condens. Matter. **11** (1999), 10041 – 10046.
14. Masakazu Katsuno, Noboru Ohtani, Jun Takahashi, Hirokatsu Yashiro, Masatoshi Kanaya; Jpn. J. Appl. Phys. **38** (1999), pp. 4661 – 4665.

Appendix B - Equipment and Supplies

Item	**Product Number**	**Supplier**	**Uses**
AFM	Nanoscope II		Surface roughness and 3-D imaging.
Controllers	252A 250 PDR-C-1B	MKS	Pressure control and display; MFC set points
Dicing Saw	DAD-2H/6TM	Disco	Programmable for dicing specific size samples
Diamond Dicing Blades	ZH05-SD1500-N1-50	Disco	Diamond coated, high speed nickel blades for dicing SiC, sapphire, ect.
UHP Ar H2 UHP 1%Ethane in Ar		Lindweld	Reactant and carrier gasses
Hydrogen Purifier	HP-50	Johnson Matthey	Purifies hydrogen to 99.99% purity
Methyltrichlorosilane		Fisher Science	Precursor, imputity concentration ~0.01%
Mass Flow Controller	C11-14995	Unit	Used to maintain constant gas volumetric flow rates
Optical Microscope	N504 115034	Nikon	Optimal and transmission imaging of substrates and epitaxial films

Optical Pyrometer	O53722	Omega	Resistive heating element temperature monitor.
Plasma Sputter Coater	Hummer VI	Process Materials Inc.	Sputter coating of non-conductive surfaces with a conductive material.
Power Supply	DCS 40-75	Sorensen	Power supply for resistive heating element. Capable of 45 volts and 70 amps max.
Pumps	E2M40 Turbo V-70	Edwards Varian	Purging of reactor for removal of possible impurities.
SEM/EDS	S-3400N	Hitachi	Imaging of surface morphology and epitaxial growth thickness
Ultrasonic Cleaner	8848	Cole – Parmer	Cleaning of substrate
Valves	SS-4BK-VS1-K SS-4BK-V35-K 0248A	Swagelok MKS	Pneumatic open/closed valves for flow control

Appendix C - Step By Step Procedure

C.1 Sample Preparation

4° off-axis and on-axis SiC were first diced using a dicing saw and diamond Disco blades. Each wafer was diced into 10mm x 10mm substrates. Substrates were marked using a diamond scribe, on either the carbon or silicon face to indicate polarity and with a mark to determine major and minor axis. Samples were then cleared of dust, fragments and oils by boiling them in trichloroethylene, TCE, for ten minutes. Samples were then rinsed with acetone to remove excess TCE, submerged in ethanol ultrasonic bath for five minutes, rinsed with water to remove remaining organics and blown dry with nitrogen. Samples weight was measured using a analytical balance, for calculation of growth thickness.

C.2 Sample Loading and Purging

After cleaning samples were loaded on a custom made resistive graphite heating element, figure. The heating element was designed to exceed temperatures of 1800 ºC by changing the cross-sectional area and path length. A 15mm x 12mm rectangle was bored from the center, to house the substrate and to help ensure even heating along the surface of the substrate. Due to the larger size of the bored region, additional scrap piece were placed around the substrate to center it.

The system was purged twice by first evacuating using an Edwards E2M40 mechanical pump to approximately 200 millitorr, then back filling to 800 torr, using ultra high purity argon, UHP. The choice of using argon instead of nitrogen was to help reduce the presence of nitrogen, which acts as a dopant and impurity in the epitaxial film. After purging, ultra high vacuum, $\sim 10^{-7}$ torr, was achieved running a Varian turbo pump, overnight.

C.3 Hydrogen Etching

Dry hydrogen etching was preformed in situ, using hydrogen purified by a Johnson Matthey HP40. It was determined, by AFM roughness, that the optimal conditions for hydrogen etching are: 2 slm hydrogen at 800 torr and 1600 °C. Each sample was etched for 10 minutes

prior to epitaxial growth. The purpose of hydrogen etching was to remove polishing scratches and other defects that may promote defects and uneven epitaxial growth.

To hydrogen etch, the reactor was filled to 800 torr, with hydrogen at 2 slm, which was maintained using a pressure transducer and butterfly valve. The reactor was then rapidly heated, ~1 minute, to temperature and allowed to etch for 10 minutes. For etching experiments, the reactor was rapidly cooled, 30 seconds, to prevent further etching. The reactor was then purged of hydrogen and filled to atmospheric pressuring using argon. Epitaxial procedure is explained in the next section.

C.4 Epitaxial Growth

After dry etching the sample, the reactor pressure was immediately reduced to 200 torr and the flow rate adjusted to epitaxial conditions, such as 1 slm hydrogen and 1 slm argon. Hydrogen flow was bubbled through the MTS bubbler allowing saturation, and carried through the by-pass line. The temperature was then increased to, 1500 °C to 1800 °C, and allowed to sit for 10 minutes or until the temperature stabilized. The MTS was then turned on for 60 minutes. At the end of the growth run, the MTS was turned off and allowed to sit for 10 minutes to ensure no reactants remain in the reactor. The reactor was then rapidly cooled, ~30 seconds, and filled to atmospheric pressure with argon.